Journal of Sound and Vibration 329 (2010) 3972–3998

Contents lists available at ScienceDirect

Journal of Sound and Vibration

journal homepage: www.elsevier.com/locate/jsvi

Experimental study of the nonlinear dynamic characteristics of suspended taut steel cables using a 3-D motion analysis system

Jiazhu Hu [a], P. Frank Pai [b,*]

[a] Black & Veatch Corporation, Overland Park, KS 66210, USA
[b] Department of Mechanical and Aerospace Engineering, University of Missouri, Columbia, MO 65211, USA

ARTICLE INFO

Article history:
Received 28 January 2009
Received in revised form
11 March 2010
Accepted 7 April 2010
Handling Editor: M.P. Cartmell
Available online 1 May 2010

ABSTRACT

This paper presents an experimental study of the nonlinear dynamic characteristics of taut steel cables using a 3-D motion analysis system. In the experiment, the taut cables have one end fixed and the other end subject to harmonic vertical excitation. The 3-D motion analysis system can simultaneously record (with high resolution) the instant 3-D coordinates of the multiple markers fixed on a vibrating cable; this distinguishes it from other experimental systems used in vibration studies, in which the vibration of only one single point can be recorded during each individual testing. With the 3-D motion analysis system, this experimental study presents a distinctive interpretation of the dynamic characteristics of taut cables in spatial domain (based on the mode-shape information of the entire cable), in addition to one in time domain (based on real-time traces of one single point). This paper introduces the 3-D motion analysis system and experimental setup, discusses practical experimental procedures, and presents a detailed analysis of three sets of experimental vibration data of three taut steel cables with different small sags. The frequency response curves were obtained for three cables. For one of the three taut cables, more informative vibration data were recorded; this cable was studied in greater detail via modal analysis using a modal decomposition technique and nonlinear time-series analysis.

1. Introduction

Cables and strings are one-dimensional structures that can sustain only longitudinal tension loads because they have negligible flexural, torsional and shear rigidities, and zero buckling loads. According to the linear theory of cable vibration [1], string and cable are, in effect, the same one-dimensional structures and the only difference lies in having a small or relatively large elasto-geometric parameter value. A taut string is a cable subject to significant external tension; the sag-to-span ratio is close to zero and, therefore, the elasto-geometric parameter is also close to zero. A cable is a string with non-zero sag and corresponding non-zero elasto-geometric parameter. As the value of the sag and corresponding elasto-geometric parameter increases, the structure's dynamic characteristics change from that primarily composed of string to that of cable. In this paper, the studied taut cable refers to a string with small sag and the $\kappa/\pi \ll 2$, where κ is the elasto-geometric parameter widely referred in loose cable vibration studies. According to linear theory of cable vibration, such a cable has dynamic characteristics similar to that of both string and cable. For a cable with small sag (a sag-to-span ratio of less than 1/8) and $\kappa/\pi \approx 2$, according to linear theory of cable vibration, various resonant vibrations are expected.

* Corresponding author. Tel.: +1 573 884 1474.
E-mail address: paip@missouri.edu (P. Frank Pai).

0022-460X/$ - see front matter © 2010 Elsevier Ltd. All rights reserved.
doi:10.1016/j.jsv.2010.04.006

Most studies on cable and string vibration, both theoretical and experimental ones, have been focused on either tightly tensioned string or loose cable with multiple resonant vibrations; few works have been conducted on taut cable (small sagged string). Although not "technically" string (and it should be noted that the dynamic characteristics of both string and cable are anticipated), taut cable behaves more like a string, according to linear cable vibration theory. However, as a result of existing sags, nonlinear behaviors caused by quadratic nonlinearities are also noted.

Research on string vibration has a long history, and there are many publications on both theoretical and experimental studies regarding various aspects of this topic. Since the early 20th century, string vibration, observed most commonly in musical instruments, has attracted the interests of many researchers. C.V. Raman, the Nobel Prize Laureate, conducted important research and made significant contributions to this field. He performed thorough investigation on the vibration of string with one end fixed and the other end subjected to periodic longitudinal excitation. This excitation was supplied by an electrically maintained turning-fork oscillation that periodically varied the string tension [2–5]. Raman's observations focused primarily on two aspects of the response. The first aspect was the maintained resonant transverse vibration. By adjusting the tension in the string and, therefore, the commensurate relationship between the natural frequencies of the string and its excitation, profiles of the maintained vibration, as well as the frequency and phase relationships between the longitudinal excitation and transverse response were investigated through both theoretical and experimental studies. Multiple resonances when the periods of the forces were integer times of the half of that of the system were observed. Single degree-of-freedom resonant vibration, compound vibration, and transitional-type vibration were recorded and studied. The second aspect was the oscillation of the fictitious node (so-called because the node is not actually absolutely at rest). Its amplitude and phase relationships to those of the rest of the string were investigated through stroboscopic studies. It was determined that the node actually oscillates parallel to the string through a certain range; the oscillation of the node has a quarter cycle phase difference from that of the string. Depending on the tension of the string and the excitation, the transverse vibration trajectory of the fictitious node may be a straight line, flat parabola, etc. Raman also worked on the acoustics of string musical instruments [6]. He worked out the theory of the transverse slip-stick vibration of bowed strings, on the basis of superposition velocities. This explanation of bowed string vibration is superior to Helmholtz's approach. However, Raman's work was based on some questionable assumptions that subsequent studies have investigated further. Woodhouse and Galluzzo [7] recently published a review of the friction-excited vibration of bowed strings.

Johnson and Bajaj [8] and Bajaj and Johnson [9] are two of the many excellent works recently published on theoretical studies of nonlinear string vibrations. The authors performed extensive bifurcation analyses of nonlinear string vibration and predicted the existence of saddle-node, period-doubling, and quasi-periodic torus-doubling bifurcations of the Hopf branch, and the appearance of chaotic attractors as well as their disappearance due to the boundary crisis. Many representative experimental studies have also been performed on string vibrations. Intent on examining the influence of different damping values, Molteno and Tufillaro [10] performed a detailed experimental study of the nonlinear dynamics of a nonmagnetic tungsten string driven by distributed forces produced by sinusoidal current stay in a permanent magnetic field. The vibration of a single point on the string was detected by an infrared photodiode that was coupled to a matched infrared phototransistor. Theoretically predicted interesting nonlinear phenomena, as presented in various works [8,9], such as quasi-period motion (both of Hopf and isolated branches), intermittent transition to chaos and boundary crisis, were observed. Some more complex phenomena not present in the theoretical study were also observed. It was demonstrated that the experimental results qualitatively agree with the predictions obtained by averaged equations for large damping cases. Nayfeh et al. [11] studied the nonlinear response of a taut string subjected to combined parametric (longitudinal) and external (transverse) excitations using multiple-scale analysis. Studies have shown that theoretical and experimental results are in agreement regarding frequency response predictions for cases where the parametric excitation is not present. However, it is likely that longitudinal motion contributes significantly to the response to parametric excitation; therefore, it is recommended that a further theoretical study which includes resonant longitudinal responses be conducted.

Research on cable vibration is dependent on such things as the configuration of the cable, the properties of the cable material, external excitation characteristics, and boundary conditions. One scenario that has been widely studied is the resonant vibration of elastic sagged non-inclined cable subjected to external (either distributed or at boundaries) harmonic excitation. Resonant vibrations are expected for cables that have crossover commensurate frequency based on linear cable vibration theory. A taut cable does not have commensurate frequencies as cables with $\kappa/\pi \approx 2, 4, 6, \ldots$; thus, few studied have been performed. However, such research work would be helpful to bridge the gap between the research on string and cable and to evaluate the influences of both quadratic (due to curvature) and cubic (due to stretching) nonlinearities on their nonlinear dynamics. There are many other valuable aspects of this work. Although lots of experimental research have been performed on string and cable vibration, because of the limitations of the experimental apparatus, none of these research have been based on the vibration data of an entire string or cable. Most recent works on string and cable vibration have been based on experimental data recorded in time domain for only one single point on the structure. Investigation using experimental data of a single fixed point on the string or cable can show the nonlinear response. However, the frequency response curve is constructed not on consistent response amplitude, for example, modal amplitude, but nodal vibration amplitude. Frequency response curves that are obtained by not using consistent vibration amplitude reflect a distorted nonlinear phenomenon, such as a hardening effect, of the system. Moreover, investigations using experimental data of a single fixed point on the string or cable cannot record and study the modal transition as the change of excitation

frequency and the compound modal vibration. This is emphasized further if the study is to investigate the dynamic characteristics in a relatively wide frequency range. The frequency response curves in this paper were plotted using responses of a fixed single point on the taut cables. The reason to for this arrangement is that the taut cable's nonlinear responses (composed of a specific single mode) were mostly within a narrow frequency interval, and, therefore, the responses at a fixed single point were acceptable for response curve plotting. However, since the obtained vibration data set recorded vibrations of the entire taut cable, the authors obtained multiple nonlinear response curves based on the response amplitudes of different locations by doing only one set of experimental testing; thus, the selective presentation of nodal responses was possible. A practical approach for experimental study of taut cable vibration using the 3-D motion analysis system is introduced and examined in this study. The state-of-the-art 3-D motion analysis system, an effective and efficient experimental testing approach, and straightforward experimental data analysis and presentation all contribute to a unique examination of taut cable vibration. A loosely sagged cable can be easily obtained by loosening a taut cable. The experimental vibration study of sagged cable is similar to that of taut cable in many aspects. For the experimental study of cable resonant vibration, response curve plotting based on consistent modal amplitude is a must, because of the prevailing existence of resonance through which multiple modes interact with one another. The experimental study of a loose cable's resonant vibration using the same experimental setup will be examined in a subsequent paper.

Perturbation methods are effective for investigating the dynamic characteristics of weakly nonlinear responses to excitations within a narrow range of specified natural frequencies. Studies on string and cable vibrations using perturbation methods have been primarily focused on responses to excitations within narrow ranges of selective natural frequencies. Experimental studies that were intended to verify theoretical predictions have been accordingly narrowed to responses to excitations within the selected frequency range. It is true that the responses around resonant frequencies are of the most important interest. Responses between resonant frequencies indicate modal transitions and are also worthy of a researcher's interest. This study investigated the dynamic responses of a taut cable for a relatively wide excitation frequency range. The taut cable had one end fixed and the other end subject to periodic excitation. The excitation was strictly in vertical direction (external type) and no longitudinal (parametric) component was included. Responses around resonant frequencies and those indicating modal transitions between resonant frequencies were all investigated. The research work was conducted using a 3-D motion analysis system; this paper summarizes the work and presents a complete picture of taut cable nonlinear vibration. The 3-D real-time vibration of the entire taut cable was recorded, and data analyses, in both time and frequency domains, were conducted. Spatial-domain analysis of the entire vibrating taut cable was accomplished on the basis of modal decomposition analysis. An unprecedented panoramic investigation of nonlinear taut cable vibration is presented herein.

2. Experimental setup and procedure

2.1. The 3-D motion analysis system

The lightweight nature of string and cable precludes the attachment of measurement sensors (e.g., accelerometers) to these structures, because the mass of the sensors may significantly influence their static and dynamic characteristics. Therefore, a non-contacting vibration measurement device is needed for the experimental investigation of the mechanics of string and cable. Fig. 1(a) shows the typical arrangement of the digital real-time 3-D motion analysis system used in this experimental study. Fig. 1(b) and (c) shows the camera and the hub of the system, respectively. The 3-D motion analysis system is useful for the noncontact measurement of significant static and/or dynamic deformations of string and cable. This system uses several (six in this study) high-resolution cameras to capture images of a structure when the retroreflective markers affixed to the structure are illuminated by lights from cameras. Using triangulation techniques [12], the known focal lengths obtained after the necessary calibrations, and the known coordinates of the markers on the 2-D images captured by the cameras, the system can automatically compute and instantly record the 3-D coordinates of the centers of each retroreflective marker. The 3-D real-time traces of all markers can be used to perform dynamic animation using stick figures to show pop-up figures of displacements and to calculate velocities and accelerations. In addition, these traces can be entered into other programs for further signal processing. The recording time length is effectively infinite, and up to 600 markers can be simultaneously traced using a computer with enough memory and a minimum 100 megabit (Mbit) data upload rate. Because the 3-D coordinates of each marker were checked and calibrated when at least two cameras observed the marker, the measurement accuracy is reasonably high. For example, measurement error is far less than 1.0 mm when the measurement volume is up to $2\times2\times2\,m^3$ The system's measurement power, ease of operation, simple setup, and extreme accuracy have made it a widely recognized experimental tool for structural vibration and dynamics study. For a more detailed discussion and other applications of the 3-D motion analysis system, please refer to Pai [12] and Ramanathan et al. [13].

2.2. Experimental setup and excitation

Fig. 2 depicts the experimental setup of a taut steel cable that was subjected to harmonic base excitations provided by a shaker. Because of the small mass of the taut cable, it could be mounted either horizontally (to avoid the effect of gravity on

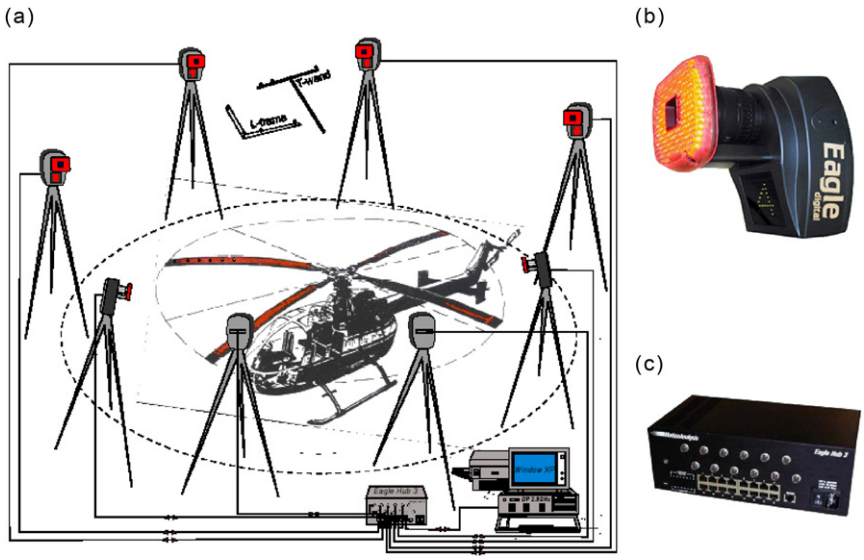

Fig. 1. The digital real-time 3-D motion analysis system: (a) typical setup of the system, (b) digital camera, and (c) hub.

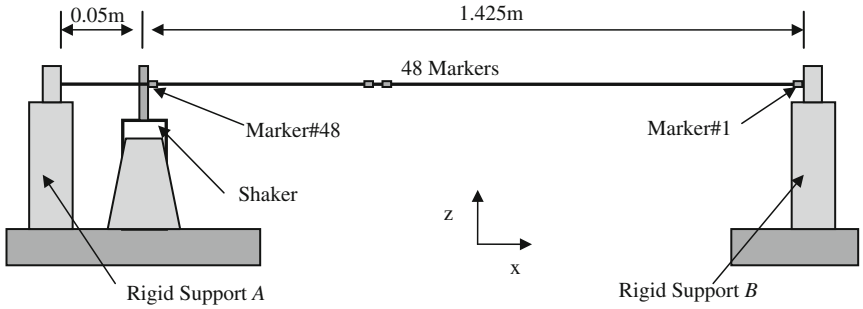

Fig. 2. The experimental setup.

the tension) or vertically (to avoid the effects of gravity on the initial curvature). In this experiment, set screws were used to clamp the taut cable to the two rigid supports *A* and *B*, which were horizontally placed approximately 1.475 m apart and were mounted on heavy weights to ensure mechanical isolation. The shaker head was attached to the taut cable at $x=0.05$ m from the left support *A*. Forty-eight 4×15 mm rectangular retroreflective markers were affixed by winding them to the taut cable; these markers were distributed evenly between the shaker and the other fixed support. Markers 1 and 48 were attached close to the supports. Marker 25 was placed close to the middle point of the taut cable between the two supports. The motion analysis system, shown in Fig. 1, made it possible to record the dynamic response of the entire taut cable instead of only one point on it. The six cameras used in this experiment were placed at different locations, approximately symmetrical with respect to the taut cable and with three on each side. Cameras were located to ensure that they had good viewing angles and that each of the 48 markers could be seen by at least two cameras on the vibrating taut cable at all times during the testing. The capture volume was set at $1.5\times1.5\times1.5\,m^3$. The system was calibrated using an L-frame and then a T-wand to define the experimental testing coordinate system *XYZ*.

The taut cable was excited using an electrodynamic shaker, which had a maximum output force of 196 N and a frequency range of 5–9000 Hz, to supply the oscillatory boundary condition at one of the two supports. The shaker-head motion was monitored by an accelerometer mounted to the shaker head. The axis of the shaker was vertical and perpendicular to the straight line connecting the two end markers of the taut cable, so that the taut cable was transversely excited only. The excitation was controlled by an accelerometer attached to the head of the shaker for feedback. The accelerometer provided feedback of the base motion to a shaker controller, which modified the ac voltage accordingly to keep the base motion harmonic. The software in the computer system controlled the entire measuring system. It tracked and identified the markers and provided the XYZ coordinates of all the markers at consecutive moments of time. The data were exported in ASCII format and were then processed using the author's post-process codes (written in MATLAB).

2.3. Frequency sweeping scheme

Temporal- and spatial-domain data for the vibrating taut cable excited at a specific frequency were acquired during the test by recording the coordinates of all 48 markers on the taut cable. Because nonlinear vibration depends on initial conditions, the tests should be performed by continuously varying, either by increasing and then decreasing, or by decreasing and then increasing, the excitation parameter (either the excitation frequency or the amplitude) through the desired range of the parameter. After the first set of data was collected by continuously increasing (decreasing) the parameter value, a second set of data was collected by continuously decreasing (increasing) the parameter value. However, these kinds of sweeping tests may confuse a nonlinear transient vibration for a steady-state one, and only one type of vibration for each parameter value can be obtained. After a couple of experimental attempts, a practical frequency sweeping scheme for the experiment was developed. In this sweeping scheme, each test was stopped before the parameter (frequency or amplitude) was changed for the next test. Each test started with the same initial conditions (still taut cable); therefore, the tests were independent of the changing direction of the parameter. For the same set of experimental parameters, after one steady-state vibration was recorded, the steady-state vibration was disturbed in various ways and other potential steady-state solutions were obtained. In most cases, a stable planar response (if it existed) was obtained by exciting the initially still taut cable, and the nonplanar response was obtained by introducing a disturbance to the planar vibration. Depending on the relative stability of the planar and nonplanar responses, the magnitude of the disturbance to alter the response from stable planar to stable nonplanar varied. Typically, the disturbance for obtaining a stable nonplanar response for excitations near the theoretically predicted saddle–node bifurcation point would have a larger magnitude. This is because the initial condition space for the stable planar solution is comparatively much larger than that of the nonplanar solution. In this manner, vibrations starting with different initial conditions were simulated, and potential multiple solutions were not overlooked.

In this study, tests were performed by varying the excitation frequency only, and the excitation amplitude was held constant. For every parameter change, either increasing or decreasing, it was necessary to ensure that the transient motion had dissipated so that a steady state could be reached before the response was captured by the camera system. In general, a steady state was attained within 1–2 min after the excitation reached a steady state for the specified amplitude. It was observed that it took more time for the response to reach a steady state in those tests with parameters near where bifurcation occurred. For example, it took a longer time for the vibration to reach a steady state at approximately the point where the planar response branch and the nonplanar branch were connected. Theoretically, the step-size of increase or decrease of the parameter depends on the closeness of the excitation frequency to the bifurcation frequencies. When the excitation frequency is close to the resonant frequency, the increase step needs to be small because various nonlinear phenomena exist for this frequency range; this range can be very small and easy to be overlooked. In these experiments, the excitation frequency was increased by a 1 Hz or larger value when the frequency was far from the resonant frequency, and by a 0.5 Hz or smaller value when it was close to the resonant frequency so that it was possible to observe important phenomena (such as period-doubling, quasi-periodic and chaotic motions) that might appear. In actual application, the appropriate step-size will depend on practical experience. Usually, an initial rough screening will provide some information about appropriate step-size determination. The total number of excitation frequency increments will depend on the frequency range to be investigated and on the capacity of the experimental apparatus.

2.4. Experimental parameters

The experiments described in this paper were performed on a 1.425 m (effective length) steel wire whose diameter was 0.4572 mm (0.01 in). The taut cable was stretched with a pre-tension T that was obtained by attaching weights to the taut cable through a pulley before the taut cable ends were fixed using clamps. Because of friction, the true tension in the taut cable was smaller than that provided by the weights. Although not accurate, it should be a value with a deviation less than 1 lb, as observed. The tension had to be low enough to ensure that no yielding occurred in the taut cable, but high enough so that the initial bending deformation would not significantly affect the vibration. In addition, the maximum vibratory strain on the taut cable (which can be determined by the maximum vibrating amplitude) could not be so large as to be out of the linearly elastic range of the material. Since steel wires were used and only low-frequency vibrations were tested in this experimental study, these problems did not appear. For taut steel cable, the longitudinal wave speed c_u is much higher than the transverse speeds c_v and c_w. To reduce the inertia effect of the retroreflective markers on taut cable vibration, the diameter of the markers must be as small as possible but still visible to the cameras. A smaller marker diameter results in more accurate experimental data recording. Large markers cause image distortion and reduce the accuracy of the measured center locations (i.e., the measured or recorded center position of each marker by averaging different views from all cameras). In the experiments conducted, the diameter of the marker was approximately 1.5 mm, which is small compared to the vibration amplitude in most cases.

With regard to dynamic parameters, the natural frequencies need to be determined in order to gain a general understanding of the dynamics of taut cable. The theoretical method using material stiffness, mass density and taut cable geometry to determine the linear natural frequencies is straightforward, but can be used for reference purpose only because of the inaccuracy caused by nonlinearities and uncertain pre-tension forces, etc. Experimental approaches are preferred. The fundamental frequency of transverse vibration can be determined by the Fast Fourier Transformation (FFT)

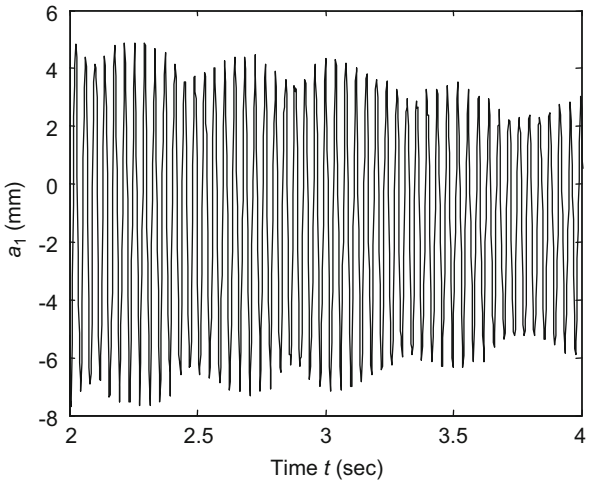

Fig. 3. The experimental data used for damping and fundamental frequency calculation.

Table 1
Parameters of Taut Steel Cable.

Parameter	Symbol	Measured/calculated values
Damping ratio	ζ (assuming ζ_v=ζ_w=ζ)	0.005–0.01
Length	L	1.474 m
Diameter	d	0.4572 mm
1st natural frequency	ω_1	17.5, 25, 17.5 Hz for the 1st, 2nd, and 3rd cases
Tension force	T	$\approx$ 8.896 N
Young's modulus	E	200×10^9 N/mm^2
Mass per unit length	m	0.0013 kg/m

analysis of the decaying free oscillation of the taut cable that was started by a small initial transverse displacement. For these experiments, the taut cable was plucked at the middle point and, therefore, the initial shape of the taut cable was a triangle consisting of many harmonics. Since the high-frequency harmonics died out quickly and only the primary harmonic was left for a longer time, the fundamental frequency was obtained by analyzing the latter part of the time-domain data. Because of the initial curvature, possible uneven gravity distribution, uncertain pluck by a finger and other reasons, the taut cable was observed to readily undergo nonplanar vibration. In these experiments, the taut cable was plucked many times until an approximately pure planar vibration was obtained and captured. The recorded data used to determinate the primary frequency and damping ratio are plotted in Fig. 3. The vibration decay observed in the experiments was smooth, and the vibration was primarily planar. After the fundamental frequency is obtained, other natural frequencies can be roughly deduced using the linear taut cable vibration theory.

The longitudinal wave speed can be determined by detecting the longitudinal motions of the markers. However, the longitudinal wave speed of the steel wire, 4000–6000 m/s, is very high and beyond the measurement capability of the motion analysis system. By assuming that exactly two frames are captured at the two instants that the elastic wave starts at one end and arrives at the other end, the maximum wave velocity $\overline{c}_u$ that can be measured by the motion analysis system with a maximum frame rate of 2000 frames per second would be

$$\overline{c}_u = L/(1/2000) = 1.425 \times 2000 \text{ m/s},$$

which is lower than the wave speed of the steel wire. Here, L is the length of the taut cable. Therefore, although this approach is theoretically possible, it is impractical for the purpose of these experiments. The damping ratio ζ was determined using the logarithmic decrement method. The system parameters identified using the methods and approaches discussed above for these experiments are listed in Table 1.

3. Experimental results

3.1. Frequency responses of three taut cables

The excitation amplitude of the shaker was set at 1 mm for frequency sweeping. The in-plane and out-of-plane response amplitudes of each marker were taken as the lengths of the major and minor axes of the elliptic trajectory obtained by

ellipse-fitting. The frequency response curve for a marker was obtained by plotting the excitation frequency with respect to the response amplitude of the chosen marker. The frequency spectrum of each marker's time trace can be obtained by FFT analysis. The three tested wires had different and virtually non-negligible sags. All of the sag-to-span ratios, however, were small and, therefore, the wires behaved like a taut cable. The upper limits of the excitation frequency range were constrained by the experimental system. Higher excitation frequencies made the system out of control when a closed loop excitation was used. This was due to the large variation in tension force acting on the shaker during the vibration. The first taut cable had a sag-to-span ratio of 1/801; its static equilibrium configurations, which were plotted using curve-fitted data and original data, are shown in Fig. 4(a). In Figs. 4–6(b, c), dots represent out-of-plane responses and circles represent in-plane responses. For the first cable, the scanning range was from 12 to 35 Hz, and only responses to harmonic excitations around the first natural frequency were examined. The in-plane and out-of-plane frequency response curves of Marker 25 are shown in Fig. 4(b) and (c), respectively. The hardening effect of the response can be observed. The second taut cable was a little more tightly tensioned, and the sag-to-span ratio was close to 1/1000. Fig. 5(a) shows the static equilibrium configurations. The examined excitation frequency range was from 15 to 53.5 Hz. The in-plane and out-of-plane frequency response curves of Marker 25 are shown in Fig. 5(b) and (c), respectively, where it can be seen that the hardening effect is more pronounced. As a result of being subjected to a larger tension force than the first and third one, the second taut cable had a larger value of natural frequency, as shown in Fig. 5(b) and (c). The third taut cable had a sag-to-span ratio of 1/756 but was still considered as a taut cable, because its elasto-geometric parameter [1,14,15] was determined to be 0.2171 (much less than 2). Therefore, it could be expected to behave more like a string or taut cable than a loose cable, although there was small sag. The testing frequency range was from 15 to 53.5 Hz. The static equilibrium

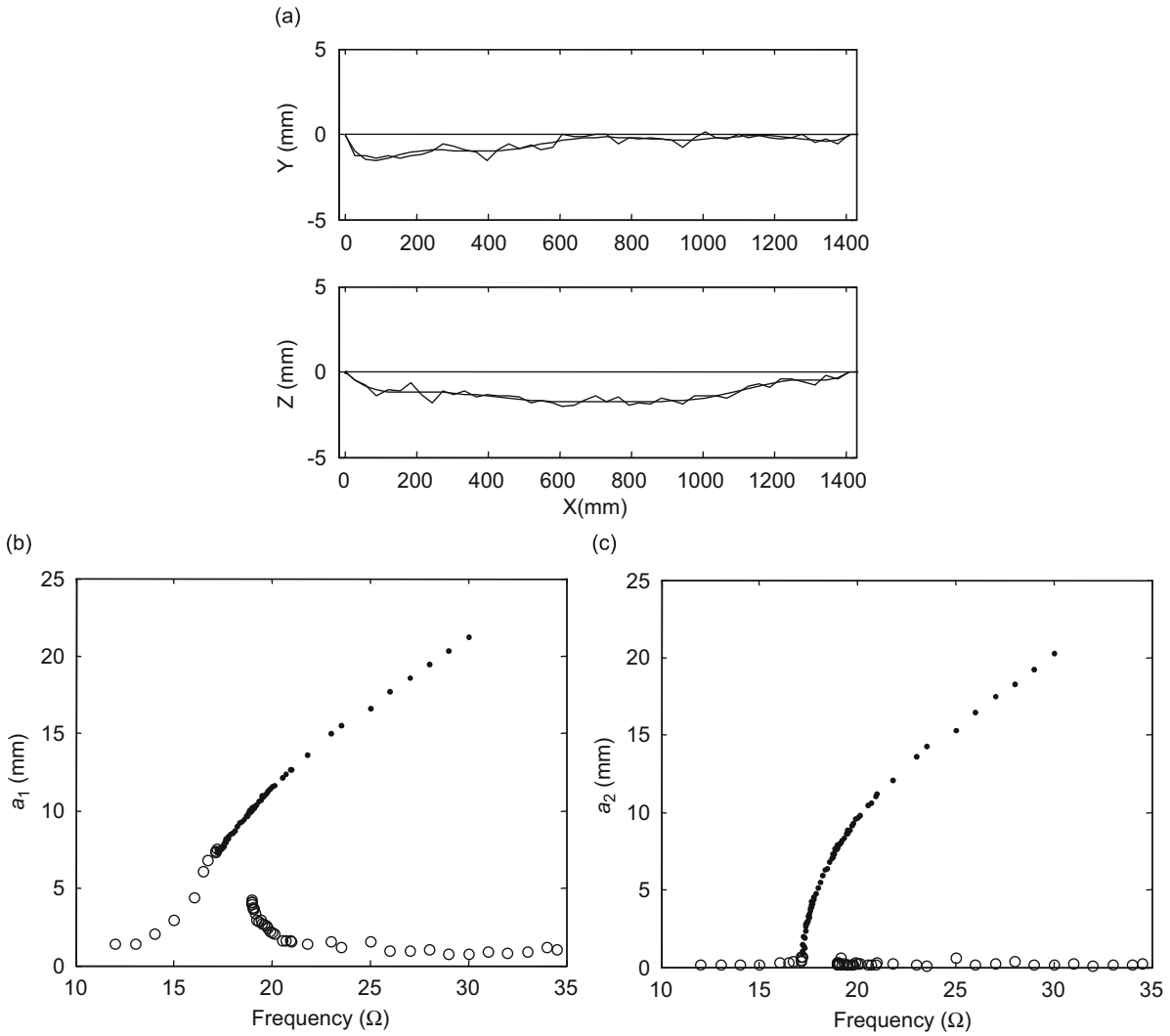

Fig. 4. The first string with a sag-to-span ratio1/801: (a) the static equilibrium configurations plotted using the curve-fitted data and the original data, (b) the in-plane frequency response curve, and (c) the out-of-plane frequency response curve of Marker 25.

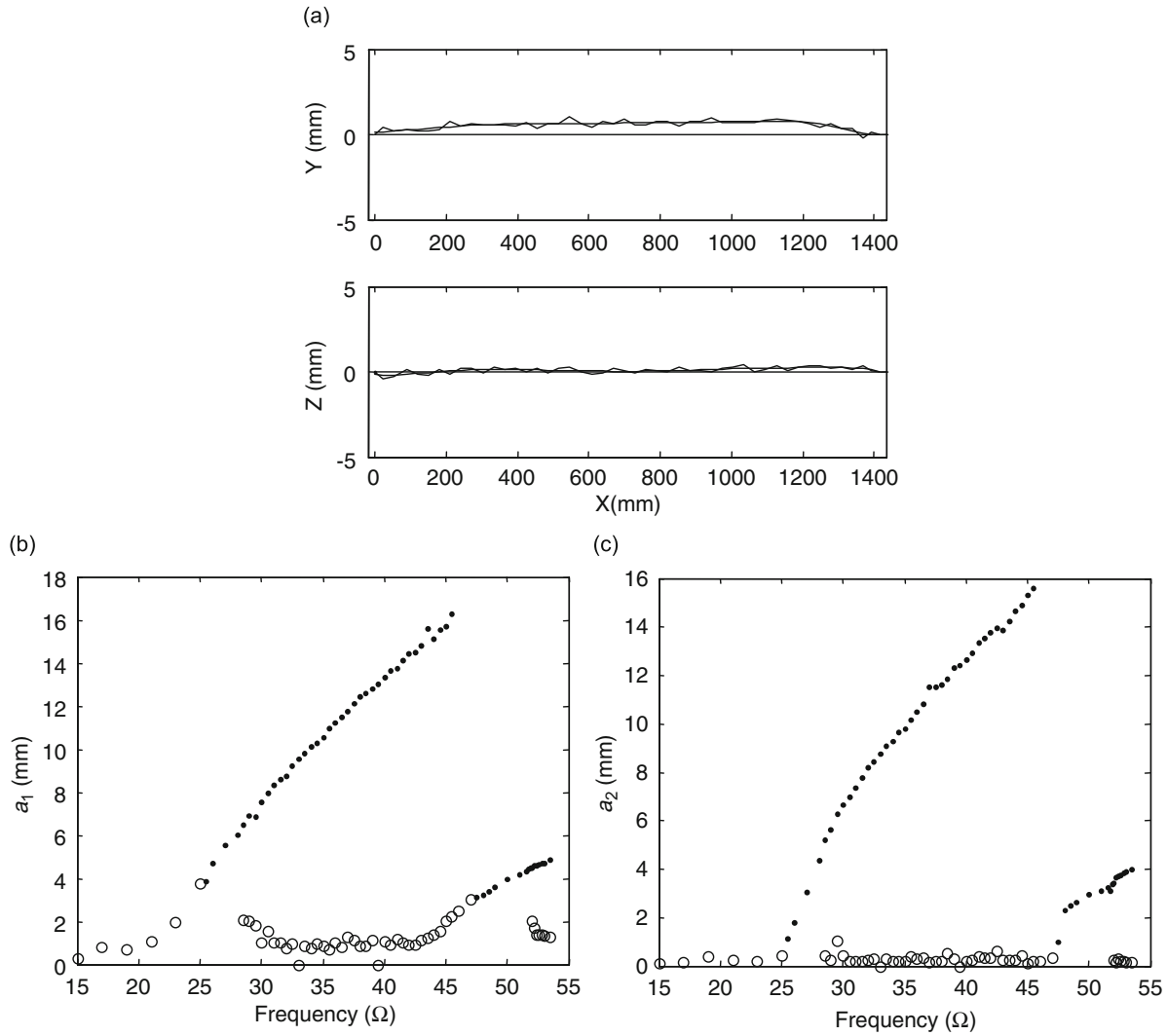

Fig. 5. The second string with a sag-to-span ratio 1/1000: (a) the static equilibrium configurations, (b) the in-plane frequency response curve, and (c) the out-of-plane frequency response curve of Marker 25.

configurations are shown in Fig. 6(a). The in-plane and out-of-plane frequency responses of Marker 9 are shown in Fig. 6(b) and (c), respectively. Marker 9 was chosen for the frequency response plot because, around this location, the third-mode vibration had peak amplitude. It was practically impossible for the experimentally recorded out-of-plane response to be completely zero even under actual planar vibration because the markers had non-zero dimensions and the marker locations that were seen and recorded by the camera system changed at different vibration instants. Consequently, some solid dots of small amplitude appeared in the plots of the out-of-plane response curves. All responses of the three tested taut cables were periodic, which was verified by their frequency spectra. No nonlinear vibrations of the period-doubled, quasi-periodic, torus-doubled or chaotic types were observed. This is probably due to the large vibration damping values; these phenomena occur only for vibrations of taut cables or strings with very small damping values.

Because the third taut cable had richer and more informative responses recorded, this study concentrated on the response of that taut cable. Based on the response characteristics, the recorded responses were divided into seven branches, which are marked as B1–B7 (B represents Branch) in Fig. 6(b) and (c). For the convenience of the following analysis, each continuous response curve was divided into planar (odd numbered branch) and nonplanar (even numbered branch) sections. The first branch B1 is the one whose response starts from a translation motion (under low-frequency excitations) to a planar vibration of the first mode (under excitations close to the first natural frequency). The second, fourth, and sixth branches (B2, B4, and B6) represent nonplanar vibrations primarily composed of the first, second, and third modes, respectively. The third, fifth, and seventh branches (B3, B5, and B7) represent planar vibration transitions in which the major participating mode changes from the first to the second, the second to the third, and the third to the fourth mode, respectively. Based on the number of different types of responses to one excitation frequency, the excitation

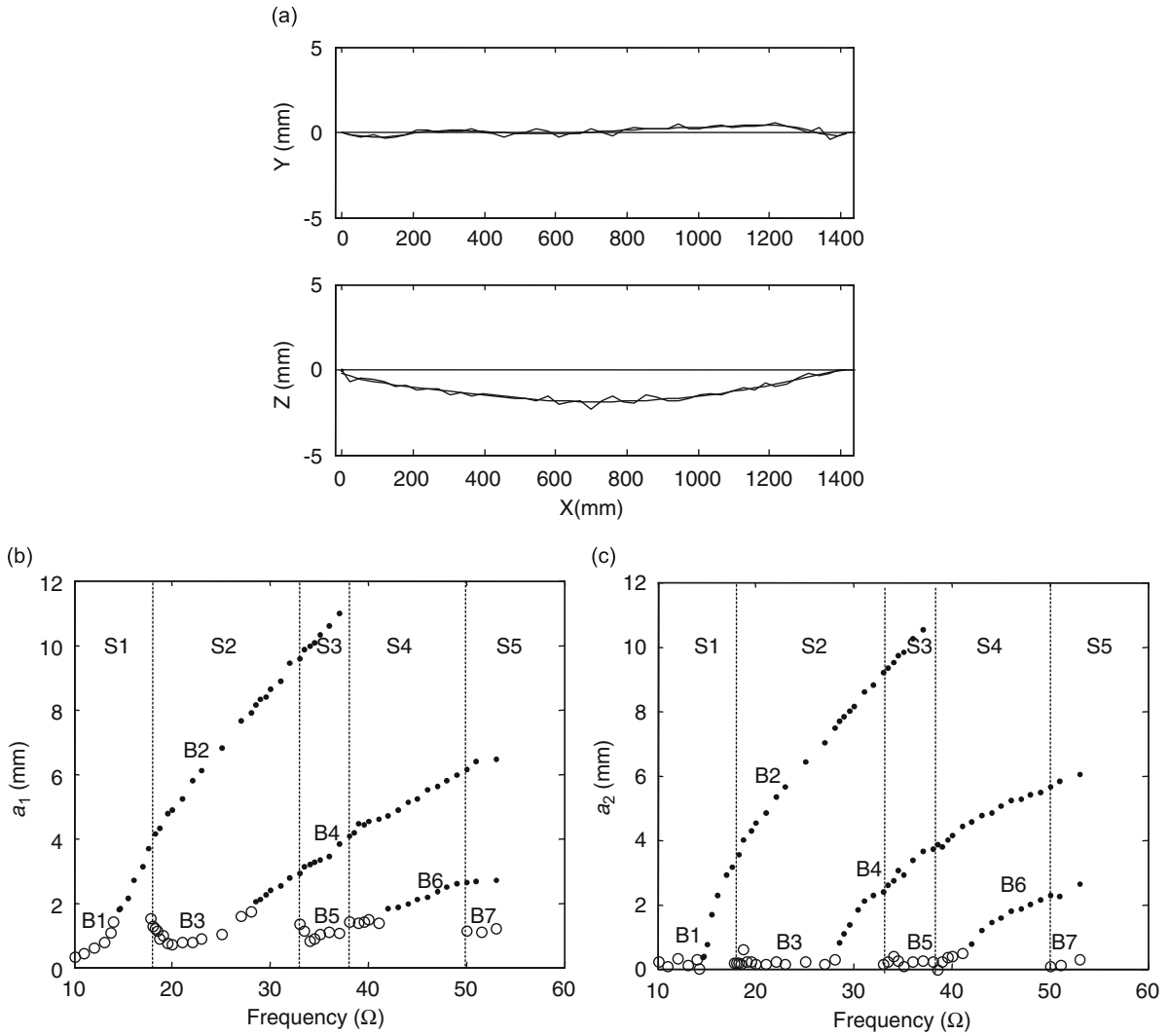

Fig. 6. The third string with a sag-to-span ratio 1/756: (a) the static equilibrium configurations, (b) the in-plane frequency response curve, and (c) the out-of-plane frequency response curve of Marker 9.

frequency range was divided into five subintervals. The subintervals are marked as S1–S5 (S represents Subinterval) in Fig. 6 (b) and (c).

3.2. Response observation for frequency sweeping

By observing the frequency response curves, the responses for increasing frequency sweeping can be summarized as follows. Initially, there was no out-of-plan vibration, and the motion was strictly planar. As the excitation frequency was increased, the planar vibration became unstable at an excitation frequency corresponding to the saddle–node bifurcation point in the theoretical prediction [8,9,14], which is just slightly above the natural frequency. The in-plane vibration lost stability and the out-of-plane vibration amplitude was no longer zero. As the whirling or ballooning motion started to appear, the trajectory changed from a vertical line to an ellipse. Fig. 7 summarizes the typical trajectories of responses of each subinterval and the branch. Reading vertically, the appearing and disappearing (gaining and losing stability) of the response of each branch could be observed. Reading horizontally, the responses to excitations within the corresponding frequency subinterval could be observed. The excitation frequency Ω (Hz), the major and minor axes r_1 and r_2 of the fitted ellipse and the frames per excitation period (*fpp*) for all cases shown in Fig. 7 are presented in Table 2. As the bifurcation occurred, the response curve was not second-order continuous because the slope decreased (refer to Figs. 4(b) and 6(b)), indicating that the input energy was no longer completely fed into the planar vibration only. As the excitation frequency was increased further, the major and minor axes of the ellipse, representing the amplitudes of in-plane and out-of-plane vibrations, increased with the minor axis, r_2, growing slightly faster than the major axis r_1. Just as the ellipse was about to

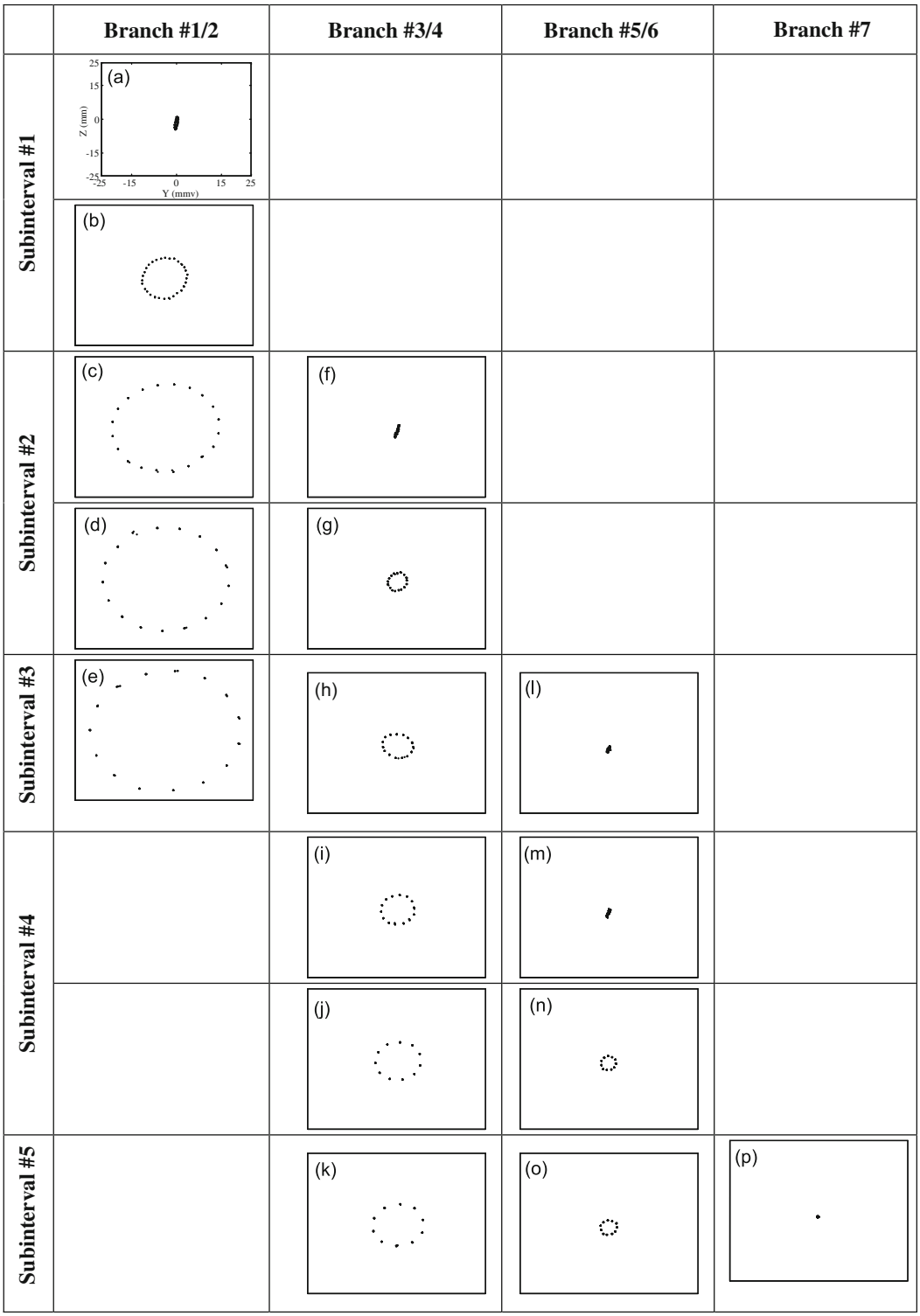

Fig. 7. The trajectories of typical responses of each subinterval and branch. The label and scale for all plots are the same as those shown in Fig. 7(a).

become a circle (i.e., $r_1=r_2$), the ballooning motion lost stability, and the hysteresis phenomenon occurred. The response to higher-frequency excitations actually depends on the properties of the taut cable. After the hysteretic frequency, corresponding to the reverse pitchfork bifurcation point in the theoretical prediction [8,9,14], the only stable response is a planar vibration of the next mode of small amplitude. However, in this study, there were two types of responses after the

Table 2
Parameters for Fig. 7 plots.

Figure	Ω (Hz)	r_1 (mm)	r_2 (mm)	*fpp*
(a)	14.2	0.53	2.84	36
(b)	17.5	6.16	7.29	30
(c)	28	14.79	15.67	20
(d)	32	17.67	18.43	17
(e)	37	20.94	21.61	15
(f)	28	0.30	2.19	20
(g)	32	2.62	3.29	17
(h)	37	4.05	4.60	15
(i)	40	4.74	5.26	14
(j)	49	6.39	6.81	11
(k)	53	7.20	7.45	10
(l)	37	0.31	1.16	15
(m)	40	0.32	1.54	14
(n)	49	2.08	2.54	11
(o)	50	2.29	2.61	11
(p)	53	0.29	0.93	10

hysteretic frequency: one was a planar vibration (B5) and the other was a nonplanar vibration (B4). This is because the natural frequencies of a taut cable are closely spaced, and the damping is small. Thus, the effective frequency range of each natural mode becomes wider and overlapped. These planar and nonplanar responses persist, and the amplitudes increase as the excitation frequency is increased. Observing the frequency response curve, the responses for decreasing frequency sweeping can be summarized similarly.

3.3. Responses of subintervals

Typical responses both of each branch and subinterval were examined to investigate the dynamic characteristics of taut cables. Moda1 analyses of the typical responses of each branch are presented in subsequent sections. This section concentrates on the typical responses of each subinterval. By studying the response variation between subintervals, the losing and gaining stability of one branch of response and the appearance or disappearance of one type of response as the excitation frequency changes may be revealed. The first subinterval S1 is from 10 to 17.5 Hz and there are two types of responses. The B1 (10–14.2 Hz) is a stable planar vibration and the B2 (14.5–17.5 Hz) is a stable nonplanar vibration. Both are primarily composed of the first mode. The second subinterval S2 starts at 18 Hz and has two types of stable responses. The first response is the B2, which is the nonplanar first-mode vibration. The response amplitude of this branch increases with the excitation frequency. The second typical response starts with a planar vibration consisting of the first and second modes. The amplitude of the first mode decreases and that of the second mode increases when the excitation frequency increases. This type of vibration belongs to the third branch (B3), which represents the vibration transition in which the major participating mode changes from the first mode to the second mode. At 28.5 Hz, a small amplitude in-plane vibration consisting of the first and second modes loses stability, and the vibration becomes a nonplanar one primarily consisting of the second mode (B4). The second subinterval lasts until 32 Hz. The third subinterval S3 starts at 33 Hz and lasts until 37 Hz. There are three different typical responses for each excitation frequency in this interval. Except for the two nonplanar solutions (B2 and B4) that also exist in the second subinterval, the third one is a planar response (B5), which consists of the second and third modes. At the end of this subinterval, the response of the nonplanar vibration that is composed of the first mode (B2) loses stability and disappears. The frequency around which the hysteresis phenomenon occurs (with increasing excitation frequency) is 37 Hz. The fourth subinterval (S4) starts at 38 Hz and has two types of stable responses. From 38 to 41 Hz, they are the planar vibration of B5 and the nonplanar vibration of B4. From 42 to 50 Hz, the planar response, primarily consisting of the second and third modes (B5), becomes nonplanar and mainly consists of the third mode (B6). The responses are similar to those of the second subinterval except that the contributing modes are different. The fifth subinterval (S5) is from 50 to 53 Hz. Subinterval S5 has three types of responses. In addition to the two typical responses of subinterval S4, a typical planar response primarily consisting of the third and fourth modes is added. This interval has a response similar to the third subinterval.

3.4. Responses of branches

3.4.1. Modal decomposition technique

The modal decomposition technique was used to study the typical response of each branch. The previously discussed qualitative analyses were based on real-time observations and experimental data of one particular marker on the taut cable. Within a wider excitation frequency range, hybrid modal vibrations are always expected. A modal decomposition based modal analysis [16] provides accurate participating frequency identification and also makes the identification of the

participating mode shape possible. Modal interactions such as resonances of sub-harmonics, sup-harmonics, etc., can be revealed. Although most recorded experimental responses are periodic, they are not of a single harmonic. Most vibrations consist of several modes due to linear and nonlinear modal couplings. Depending on the closeness of the excitation frequency to the neighboring natural frequencies, the contributing modes that have natural frequencies close to the excitation frequency carry different weights. Modal decomposition technique is widely used for the investigation of the contributions of participating modes in harmonic vibrations. In the low-frequency tests of these experiments, the vibrations were primarily composed of the first four modes. To investigate the contributions of the first four linear normal modes to the experimental operational deflection shapes at $t=t_k$, the following was assumed:

$$w(x,t_k)=\frac{x}{L}b(x,t_k)+\sum_{i=1}^{4}a_i(t_k)\phi_i(x), \tag{1}$$

where b is the shaker's vertical (Z-direction) displacement during excitation, a_i denotes the modal displacement of the ith linear mode and ϕ_i represents the ith linear mode shape. In the following experimental results analysis, $CZ_i(t)$ ($i=1, 2, 3, 4$) and $CY_i(t)$ ($i=1, 2, 3, 4$) are used to represent the modal displacements for in-plane and out-of-plane responses, respectively. To obtain the value of $a_i(t_k)$ by least-squares fitting, a spatial-domain error function Ex is defined. The value

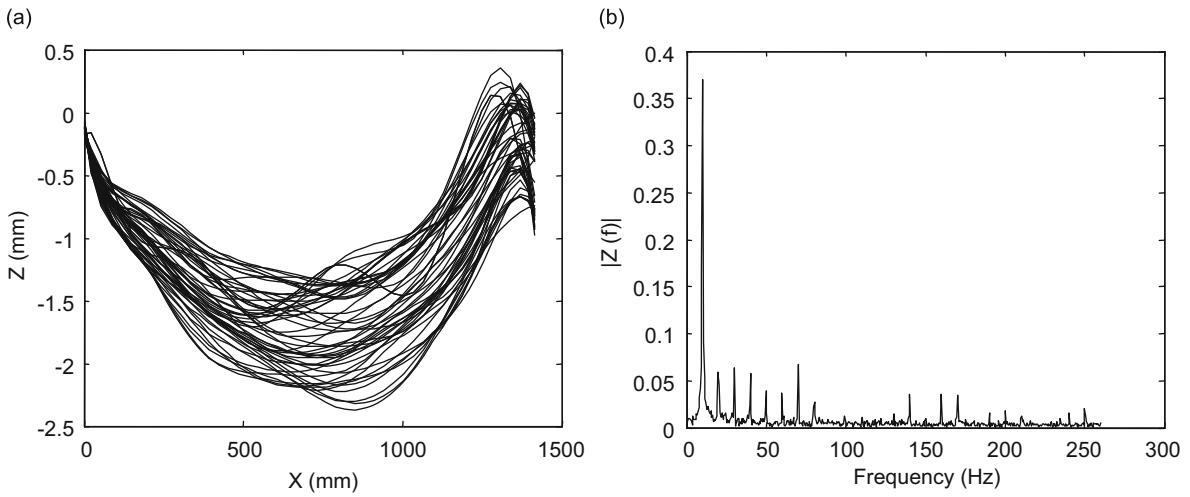

Fig. 8. Response to an excitation at $\Omega=10$ Hz: (a) 52 curve-fitted consecutive vibration profiles within 0.098 s and (b) the frequency spectra of Marker 25 Z-direction vibration.

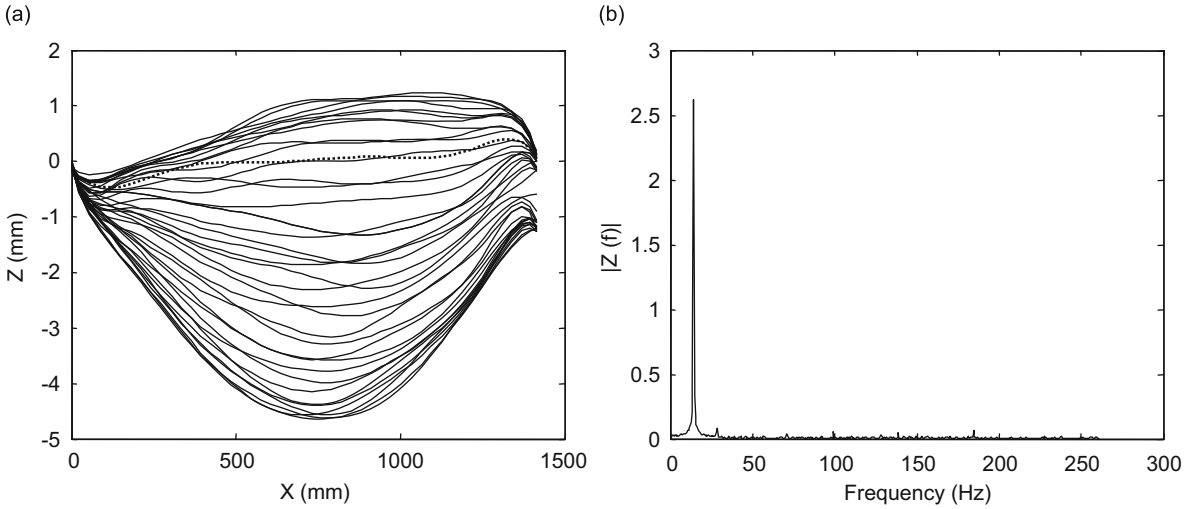

Fig. 9. Response to an excitation at $\Omega=14.2$ Hz: (a) 37 curve-fitted consecutive vibration profiles within 0.069 s and (b) the corresponding frequency spectra of Marker 25 Z-direction vibration.

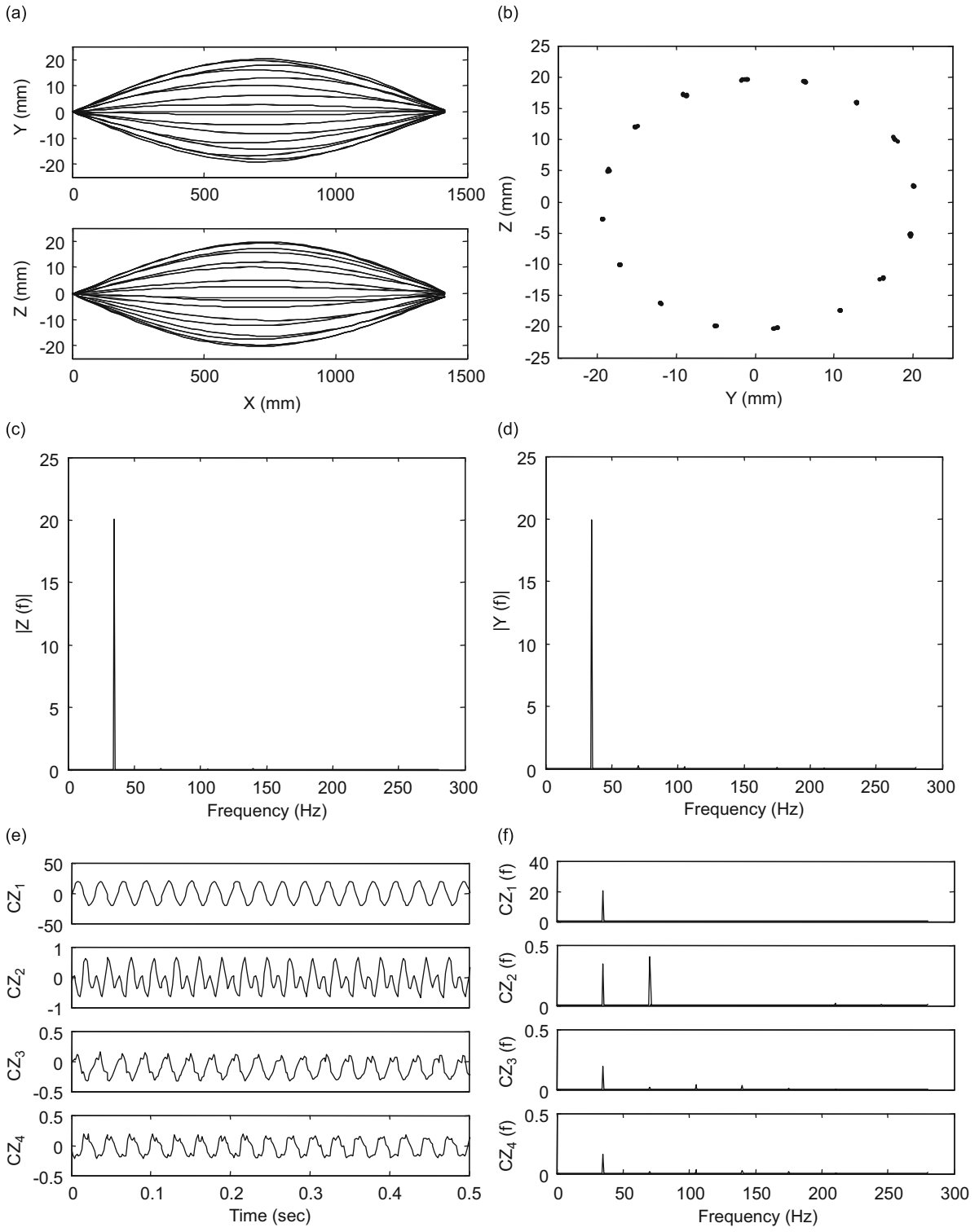

Fig. 10. Response to an excitation at Ω=35 Hz: (a) 32 curve-fitted consecutive vibration profiles within 0.055 s, (b) the trajectory of Marker 25, (c) the frequency spectrum of the *Z*-direction vibration of Marker 25, (d) the frequency spectrum of the *Y*-direction vibration of Marker 25, (e) the modal coordinates of the *XZ*-plane vibration; (f) the frequency spectra of the modal coordinates of the *XZ*-plane vibration, (g) the modal coordinates of the *XY*-plane vibration, (h) the frequency spectra of the modal coordinates for the *XY*-plane vibration, (i) error functions of the modal decomposition of the *XZ*-plane vibration, and (j) error functions of the modal decomposition of the *XY*-plane vibration.

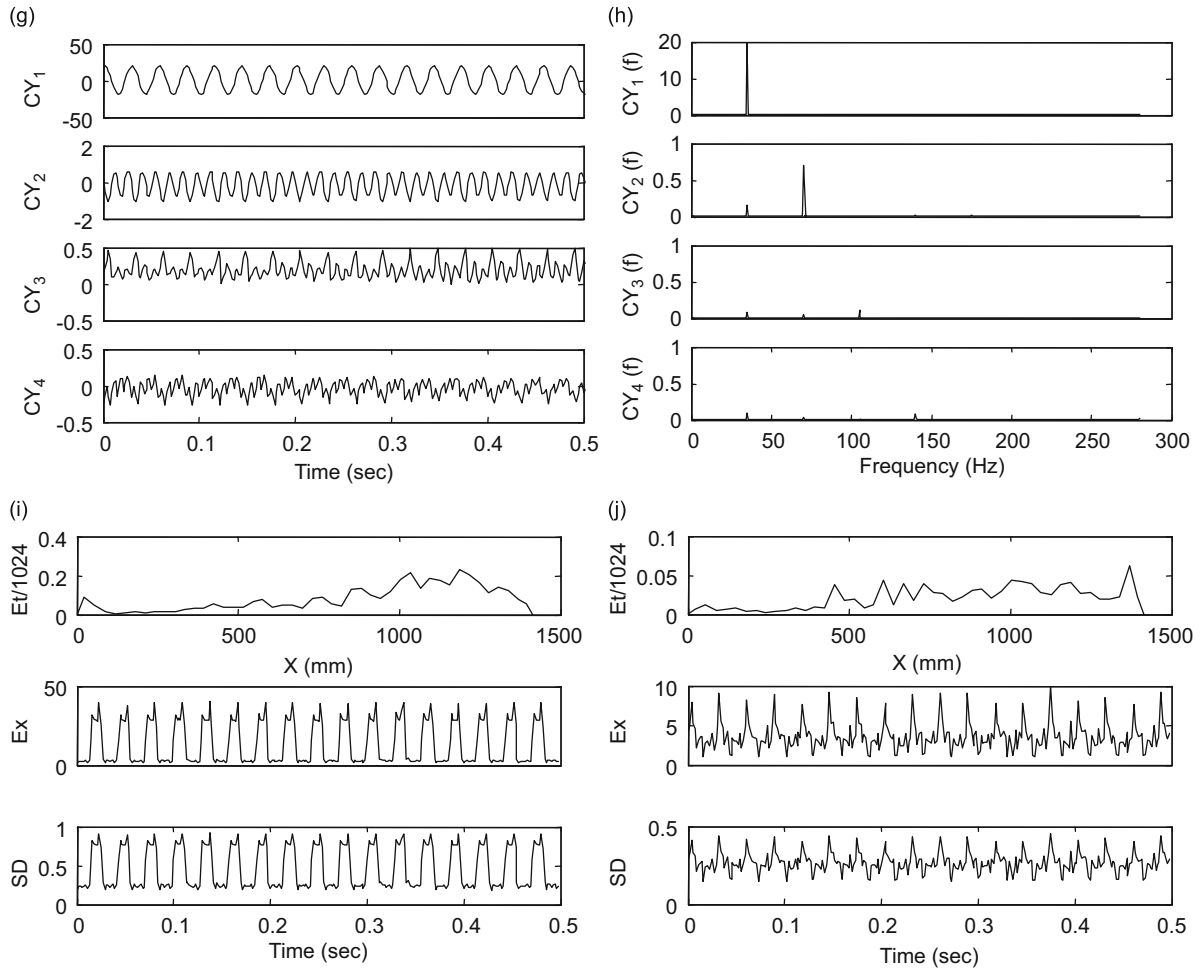

Fig. 10. (*Continued*)

of Ex at time t_k is as follows:

$$Ex(t_k) \equiv \sum_{m=1}^{nm} [w(x_m,t_k) - \hat{w}(x_m,t_k)]^2, \tag{2}$$

where $\hat{w}$ denotes experimental data. $t_k (k=1, \ldots, N)$ are the time instants of recording, and N is chosen to be 2^9 or 2^{10} for the FFT analysis. nm is the number of markers (=48 in this study). The equations for determining $a_i(t_k)$ are as follows:

$$\frac{\partial Ex(t_k)}{\partial a_i} \equiv \sum_{m=1}^{nm} 2[w(x_m,t_k) - \hat{w}(x_m,t_k)]\phi_i(x_m) = 0, \quad i = 1, 2, 3, 4. \tag{3}$$

The standard deviation, $SD(t_k)$, of the fitted displacement profile at each time instant t_k is as follows:

$$SD(t_k) \equiv \sqrt{Ex(t_k)/nm}. \tag{4}$$

Moreover, one can check the displacement of the marker at $x=x_m$ to determine how much its curve-fitted displacement $w(x_m, t_k)$ from Eq. (1) matches with its experimental one $\hat{w}(x_m, t_k)$, and this can be quantified using the following time-domain error function $Et(x_m)$. The value of $Et(x_m)$ at location x_m (marker m) for a 2^{10} time instants is as follows:

$$Et(x_m) = \sum_{k=1}^{1024} [w(x_m,t_k) - \hat{w}(x_m,t_k)]^2. \tag{5}$$

The linear combination of two modes vibrating at the same frequency and having a phase difference α is as follows:

$$\begin{gathered} \overline{w} = \overline{\phi}_2(x)\sin(\Omega t) + \overline{\phi}_1(x)\sin(\Omega t + \alpha) = \Phi(x)\sin(\Omega t + \overline{\alpha}), \\ \overline{\phi}_1 \equiv a_{1\max}\phi_1, \quad \overline{\phi}_2 \equiv a_{2\max}\phi_2, \end{gathered} \tag{6}$$

where

$$\Phi(x) \equiv \sqrt{\overline{\phi}_2^2 + 2\overline{\phi}_1\overline{\phi}_2\cos(\alpha) + \overline{\phi}_1^2}, \quad \overline{\alpha} \equiv \tan^{-1}\frac{\overline{\phi}_1\sin(\alpha)}{\overline{\phi}_2 + \overline{\phi}_1\cos(\alpha)}.$$

If the phase difference α between these two harmonics is not equal to 0° or 180°, the phase for the combined vibration, $\overline{\alpha}$, is a function of x and the combined vibration is called a complex mode. A complex mode is one in which each point of the structure has its own vibration amplitude and phase angle. Consequently, each point of the structure will reach its maximum and zero deflection positions at different time instants during the vibration.

3.4.2. Responses of the first branch (B1)

The first branch (B1) in Fig. 6(b) and (c) depicts the responses to low-frequency excitations. The vibration under low-frequency excitation was dominated by the movement of the end support because the taut cable was vibrating with small amplitude. The vibration could not be adequately captured because the response amplitude and the size of the marker (1–2 mm diameter) were close to the excitation amplitude (1 mm). Fig. 8(a) depicts the 52 consecutive curve-fitted vibration profiles within 0.098 s when the taut cable was excited at 10 Hz. As expected, the frequency spectrum of the vibration of Marker 25 (around the midpoint of the taut cable), as shown in Fig. 8 (b), is complicated because of a loose signal-to-noise ratio and multiple-mode Z-direction vibration. For a higher excitation frequency at 14.2 Hz, the motion could be determined more accurately because it had a response with a larger amplitude, as shown in Fig. 9(a), 37 consecutive curve-fitted vibration profiles within 0.069 s. The frequency spectrum of the Z-direction vibration of Marker 25 (Fig. 9(b)) is much clearer, with one major harmonic at the excitation frequency. The taut cable was still not vigorously excited, and the complex

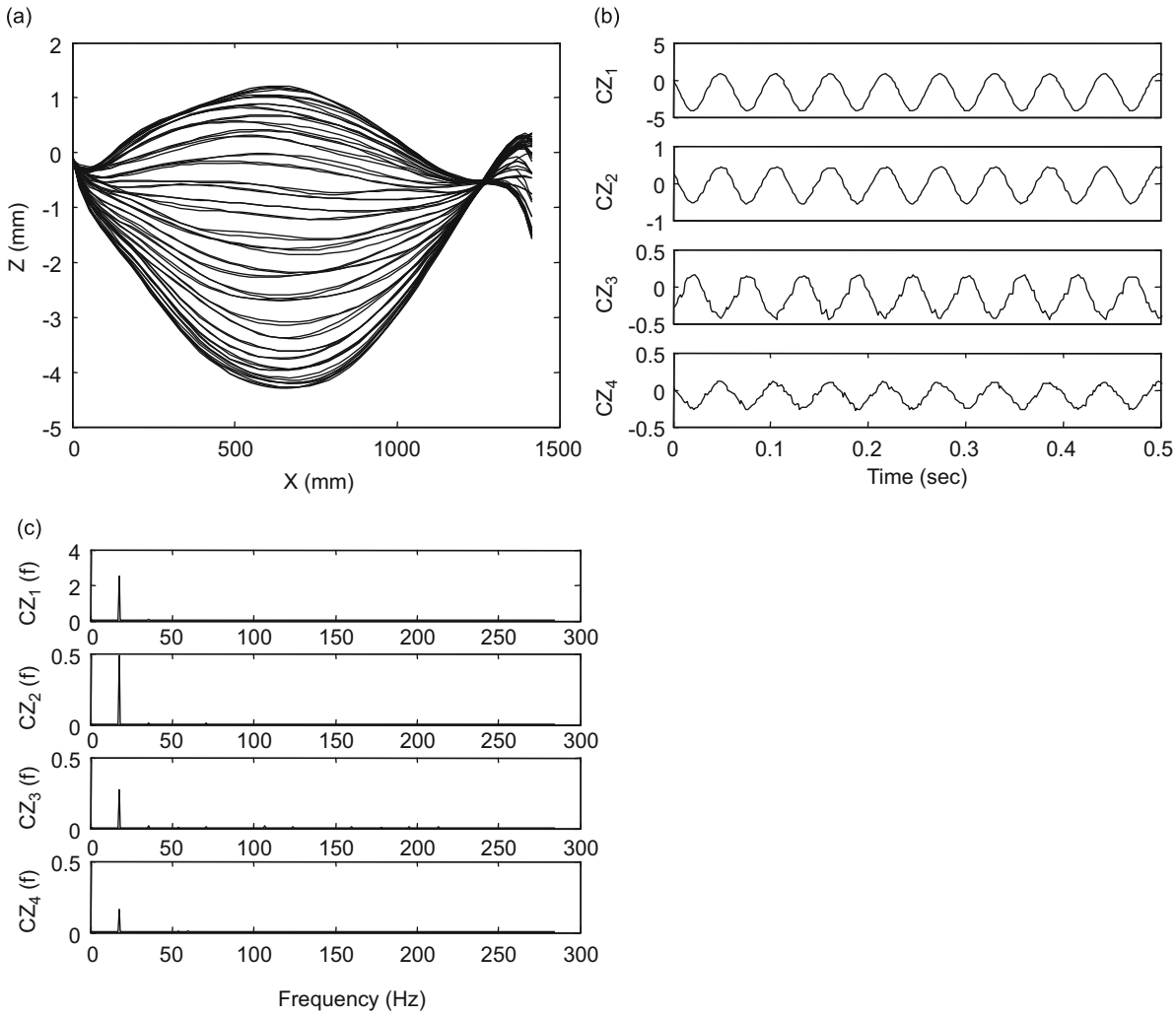

Fig. 11. Response to an excitation at Ω=17.75 Hz: (a) 64 curve-fitted consecutive vibration profiles within 0.111 s, (b) the modal coordinates of the XZ-plane vibration, and (c) the frequency spectra of the modal coordinates of the XZ-plane vibration.

behavior of the vibration was obvious. Although the largest displacement was around the midpoint of the taut cable, close examination shows that profiles at various times had different locations of maximum deflection. Traveling waves (e.g., the dotted line) can be seen in Fig. 9(a). This irregular vibration shape is the result of the interference of the incident wave that was started by the excitation with a reflected wave in a rather nonsequential and untimely manner.

3.4.3. *Responses of the second branch (B2)*

The B2 branch in Fig. 6(b) and (c) is the whirling motion primarily consisting of the first mode. As shown in Fig. 6, the amplitude of response increases as the excitation frequency increases. The 32 consecutive curve-fitted vibration profiles within 0.055 s of response to an excitation at Ω=35 Hz is shown in Fig. 10(a). The profiles are clearly separated, which indicates that the taut cable returned to the same position after a specific interval and therefore, the vibration was periodic. Close examination of the vibration profiles shows that there are exactly 16 profiles (=560(FPS)/35(Hz)). This is verified by the trajectory of Marker 25, shown in Fig. 10(b), which has 16 discrete dots, indicating that the taut cable returned to the same position after 16 frames or one vibration period. Fig. 10(c) and (d), the frequency spectra of the *Z*-direction and *Y*-direction vibrations of Marker 25, respectively, show that the periodic harmonic vibrations in both planes are exactly at the excitation frequency. Fig. 10(a) also shows that there are crossovers between the profiles. This indicates that the vibration was composed of more than one mode, though primarily the first mode. The asymmetric crossovers indicate the obvious participation of the anti-symmetric mode. The modal coordinates and corresponding frequency spectra for vibrations in two perpendicular planes are presented in Fig. 10(e)–(h). They show the existence of the second mode (first anti-symmetric mode) vibrating at both one time (Ω) and two times (2Ω) of the excitation frequency for both the *XY*- and *XZ*-plane vibrations. The Ω component is caused by linear coupling because the forcing function has a spatial distribution that is nonorthogonal to any linear modes. The 2Ω component is due to a 1:2 internal resonance. This phenomenon cannot

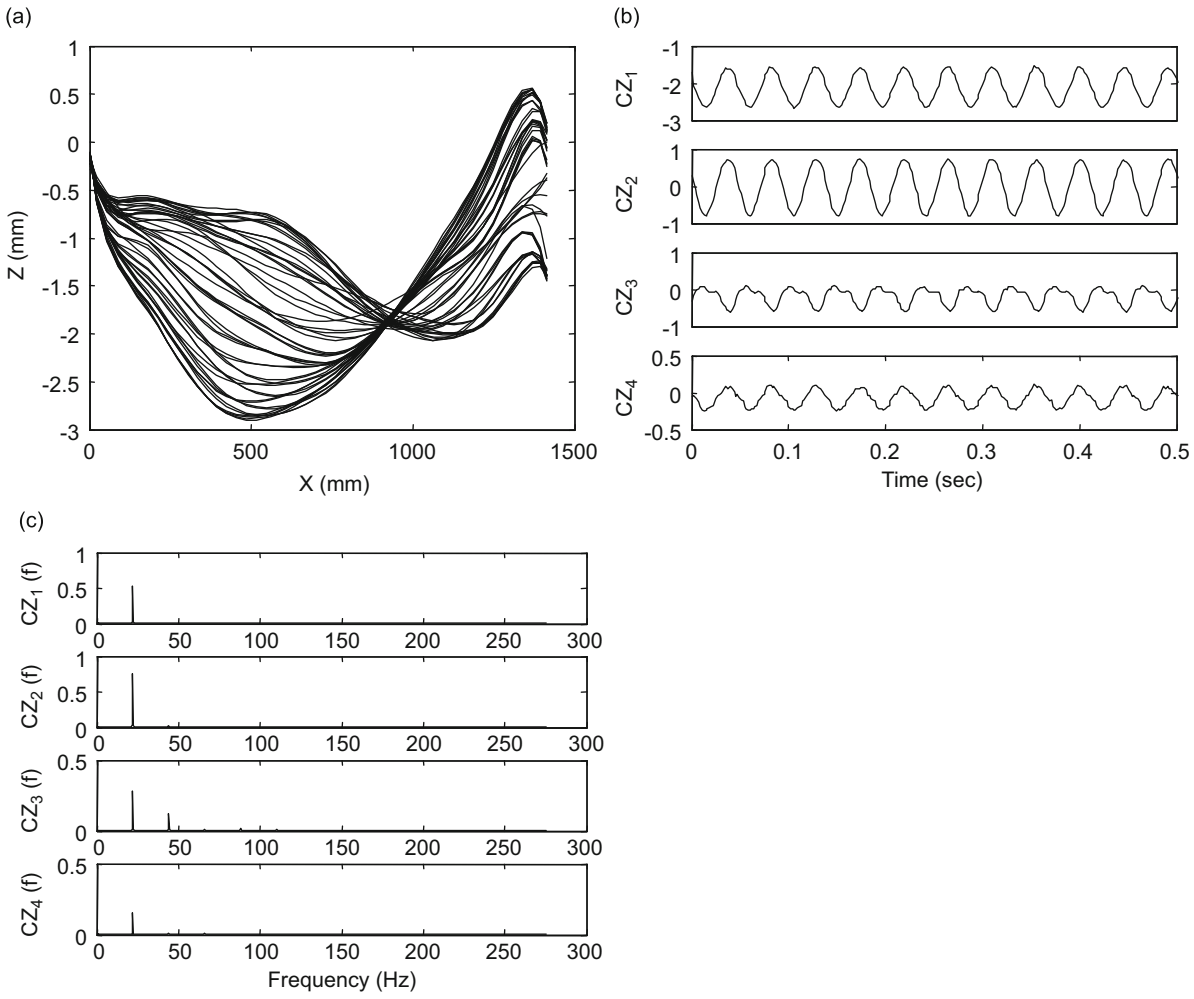

Fig. 12. Response to an excitation at Ω=22 Hz: (a) 50 curve-fitted consecutive vibration profiles within 0.089 s, (b) the modal coordinates of the *XZ*-plane vibration, and (c) the frequency spectra of the modal coordinates of the *XZ*-plane vibration.

be explained by a string model in which only cubic nonlinearity is considered. Quadratic nonlinearity due to small curvature of the sagged taut cable accounts for the resonance. Moreover, close examination of Fig. 10(a) shows that the crossovers between profiles of the *XY*-plane vibration are more serious than those of the *XZ*-plane vibration. This is because the amplitude of the 2Ω harmonic is much larger than that of the Ω harmonic (Fig. 10(h)) for the *XY*-plane vibration of the second-mode component. For *XZ*-plane vibration, the amplitudes of Ω and 2Ω harmonics have approximately the same magnitude (Fig. 10(f)). This is true for most tests on this branch, and the authors believe it is partially because of the gravity influence on the *XZ*-plane vibrations. The time-domain error function $Et(x)$ of Marker 25, the spatial-domain error function $Ex(t)$, and the standard deviation $SD(t)$ of the modal decompositions for the *XZ*- and *XY*-plane vibrations are shown in Fig. 10(i) and (j), respectively. The small values of the error functions indicate that four modes are enough for an accurate modal decomposition for this response.

3.4.4. *Responses of the third branch (B3)*

The B3 branch in Fig. 6(b) and (c) represents the transition from the first-mode planar vibration to the second-mode one. Fig. 11 shows the response when the taut cable was excited at $\Omega=17.75$ Hz. Fig. 11(a) plots 64 consecutive curve-fitted vibration profiles within 0.111 s. Fig. 12 shows the response when the taut cable was excited at $\Omega=22$ Hz. Fig. 12(a) plots 50 consecutive curve-fitted vibration profiles within 0.089 s. Fig. 13 shows the response when the taut cable was excited at $\Omega=28$ Hz. Fig. 13(a) plots 40 consecutive curve-fitted vibration profiles within 0.07 s. Together, Fig. 11(a), Fig. 12(a), and Fig. 13(a) show the obvious transition of the vibration from one primarily consisting of the first mode to one primarily consisting of the second mode. Comparing the amplitudes of the first and second modes of these cases, one can see that the first-mode amplitude decreases and the second-mode increases, indicating an increasing participation of the second mode. From the *XZ*-plane vibration modal coordinates and corresponding frequency spectra figures, Fig. 11(b) and (c) for the 17.75 Hz excitation, Fig. 12(b) and (c) for the 22 Hz excitation, and Fig. 13 (b) and (c) for the 28 Hz excitation, one can see

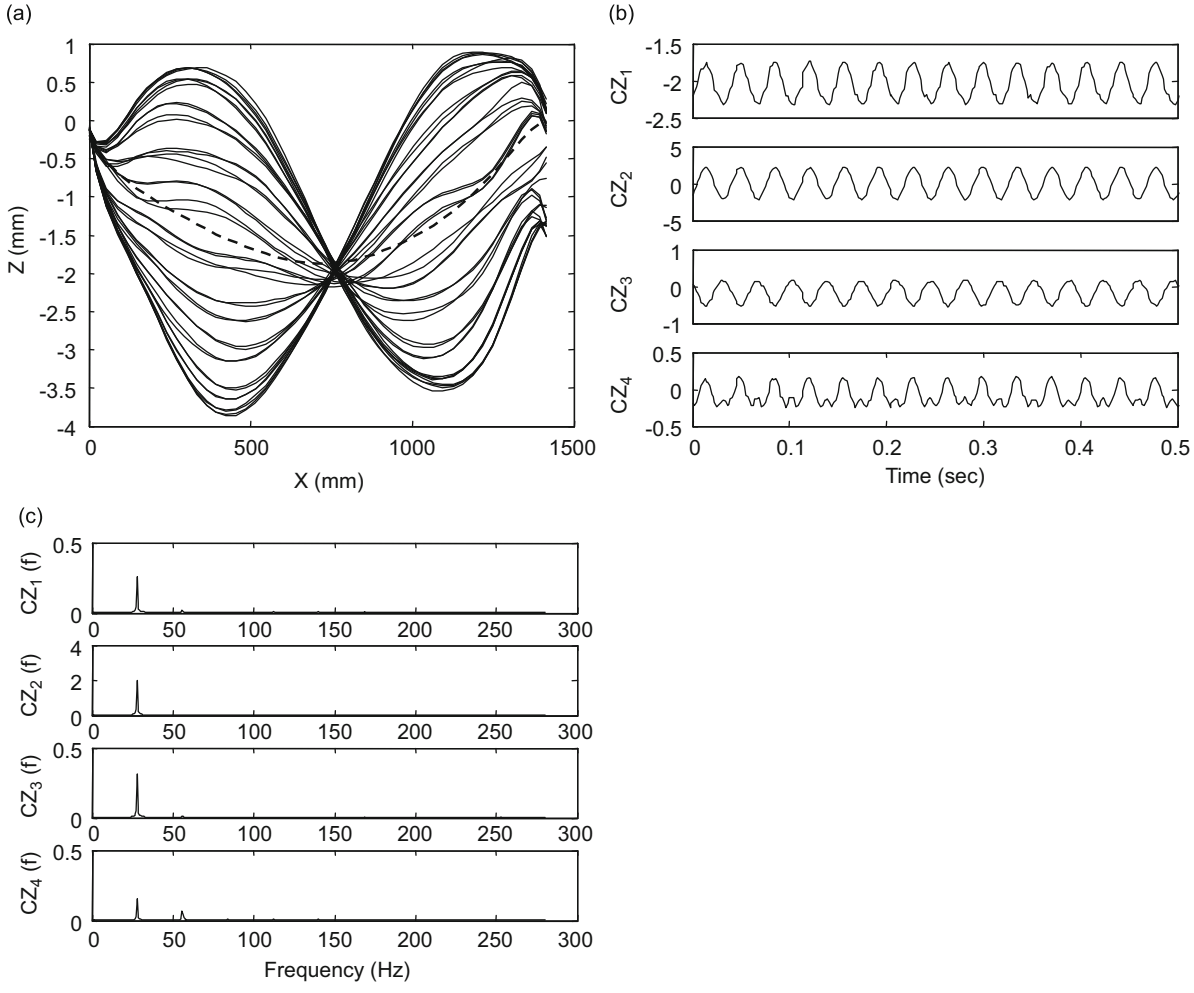

Fig. 13. Response to an excitation at $\Omega=28$ Hz: (a) 40 curve-fitted consecutive vibration profiles within 0.07 s, (b) the modal coordinates of the *XZ*-plane vibration, and (c) the frequency spectra of the modal coordinates of the *XZ*-plane vibration.

that the first and second modes are the two major components and are always in phase or have a phase difference of π for these three cases. Because of linear coupling, some higher modes had small but nontrivial amplitudes and vibrated at the excitation frequency, making the vibration somewhat complicated.

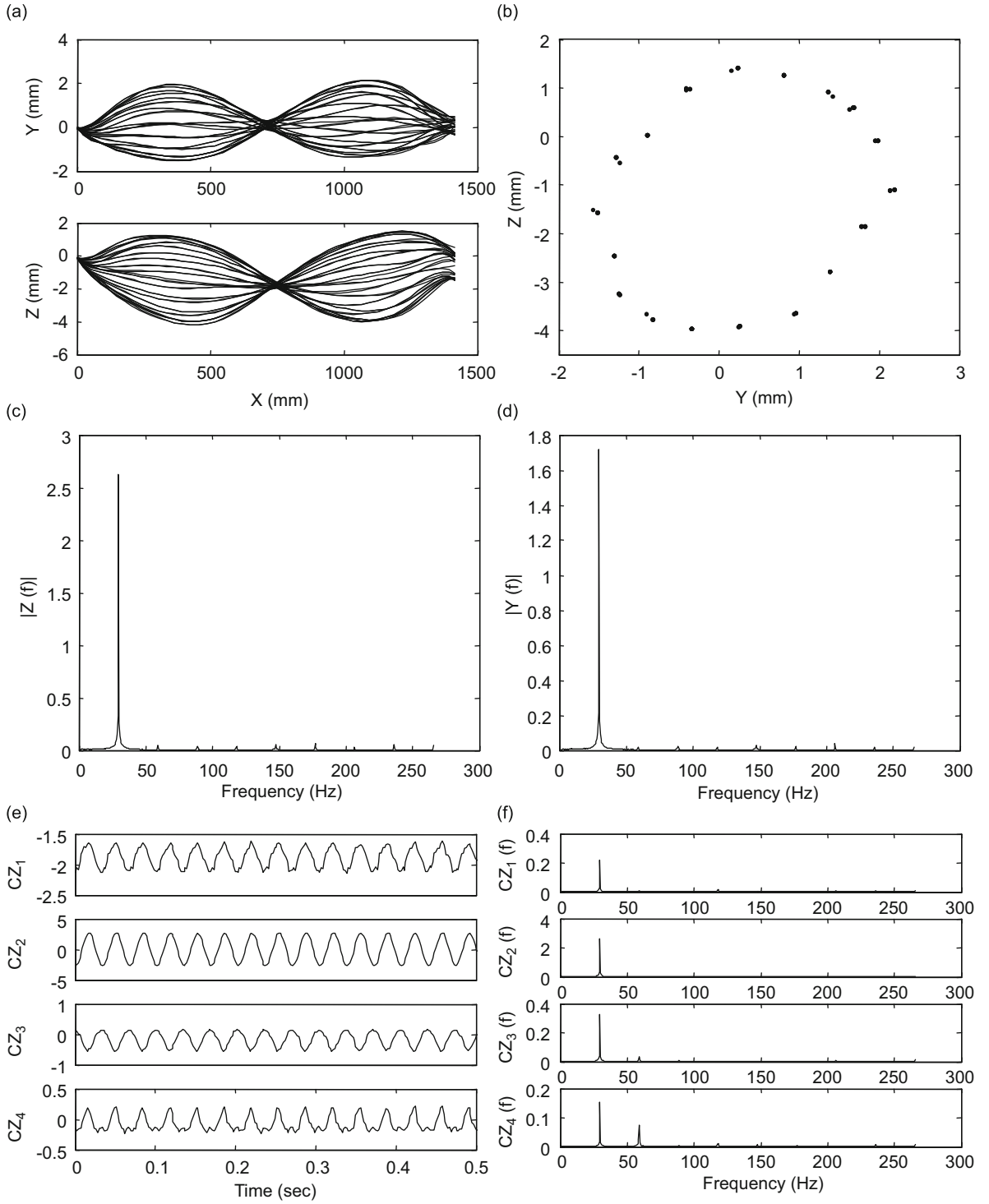

Fig. 14. Response to an excitation at Ω=29.5 Hz: (a) 36 curve-fitted consecutive vibration profiles within 0.066 s, (b) the trajectory of Marker 13, (c) the frequency spectra of the *Z*-direction vibration of Marker 13, (d) the frequency spectra of the *Y*-direction vibration of Marker 13, (e) the modal coordinates of the *XZ*-plane vibration, (f) the frequency spectra of the modal coordinates of the *XZ*-plane vibration, (g) the modal coordinates of the *XY*-plane vibration, and (h) the frequency spectra of the modal coordinates of the *XY*-plane vibration.

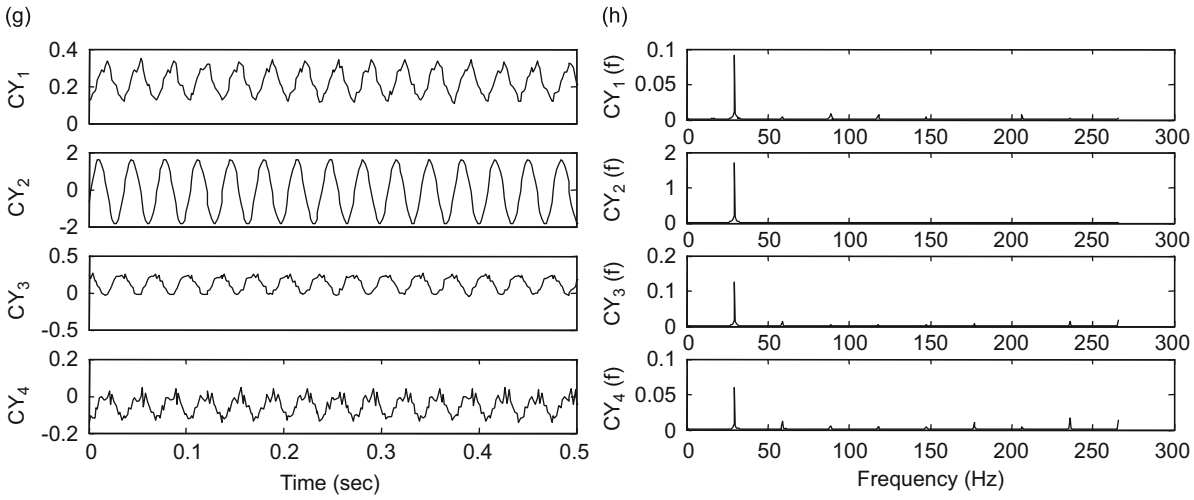

Fig. 14. (*Continued*)

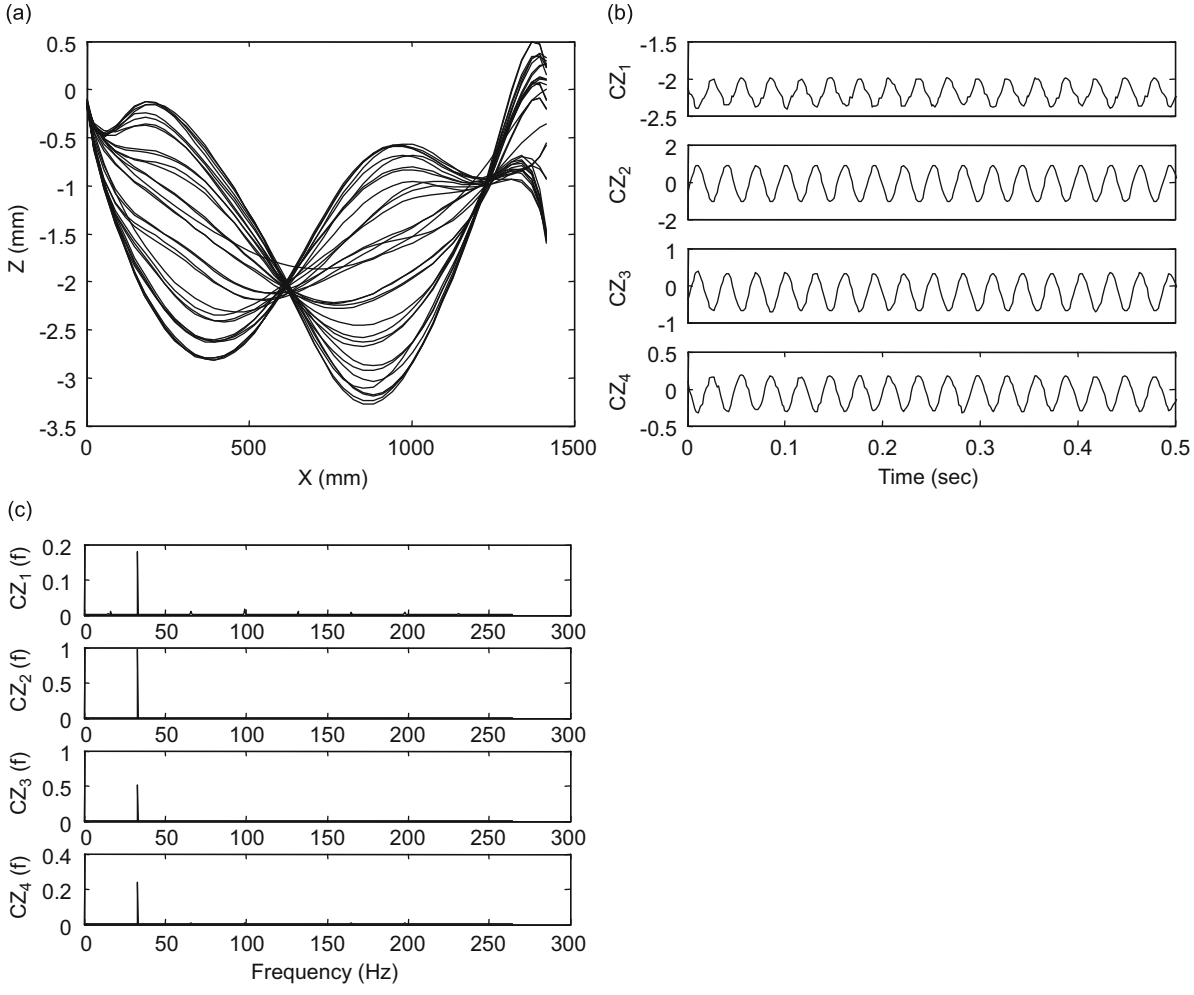

Fig. 15. Response to an excitation at Ω=33 Hz. (a) 32 curve-fitted consecutive vibration profiles within 0.059 s, (b) the modal coordinates of the *XZ*-plane vibration, and (c) the frequency spectra of the modal coordinates of the *XZ*-plane vibration.

3.4.5. Responses of the fourth branch (B4)

The B4 branch depicted in Fig. 6(b) and (c) represents a whirling motion primarily composed of the second mode. This branch has properties similar to the B2 branch. Fig. 14(a)–(h) represents plots of the response when the taut cable was excited at Ω=29.5 Hz. A plot of clearly separated 36 consecutive curve-fitted vibration profiles within 0.066 s, Fig. 14(a) indicates that the vibration was periodic. The trajectory of Marker 13 (Fig. 14(b)) has exactly 18 points, which indicates that the vibration returned to the same position after one excitation period. The frequency spectra of the *Z*-direction vibration of Marker 13 (Fig. 14(c, d)) indicate that the vibrations were periodic at the excitation frequency. Fig. 14(e)–(h) shows the modal coordinates and corresponding frequency spectra of *XZ*- and *XY*-plane vibrations, respectively. They show that the vibrations were dominated by the second mode. However, there are modes other than the second mode. Actually, it was the participation of the symmetric modes vibrating at the excitation frequency that partially made the inner node of the vibration profile unclear. In addition, participation of modes different from the second mode caused the crossover between the different profiles as observed in Fig. 14(a).

3.4.6. Responses of the fifth branch (B5)

The B5 branch shown in Fig. 6(b) and (c) represents a transition from the second-mode planar vibration to the third-mode planar vibration. It has properties similar to the B3 branch. Fig. 15 shows the response when the taut cable was excited at Ω=33 Hz. Fig. 15(a) plots the 32 consecutive curve-fitted vibration profiles within 0.059 s. Fig. 16 shows the response when the taut cable was excited at Ω=35 Hz. Fig. 16(a) plots the 32 consecutive curve-fitted vibration profiles within 0.055 s. Fig. 17 shows the response when the taut cable was excited at Ω=37 Hz. Fig. 17(a) plots 30 consecutive curve-fitted vibration profiles within 0.052 s. Fig. 18 shows the response when the taut cable was excited at Ω=40 Hz. Fig. 18(a) plots 28 consecutive curve-fitted vibration profiles within 0.048 s. From the modal coordinates and corresponding frequency spectra for *XZ*-plane vibration for each excitation shown in Figs. 15(b) and (c), 16(b) and (c),

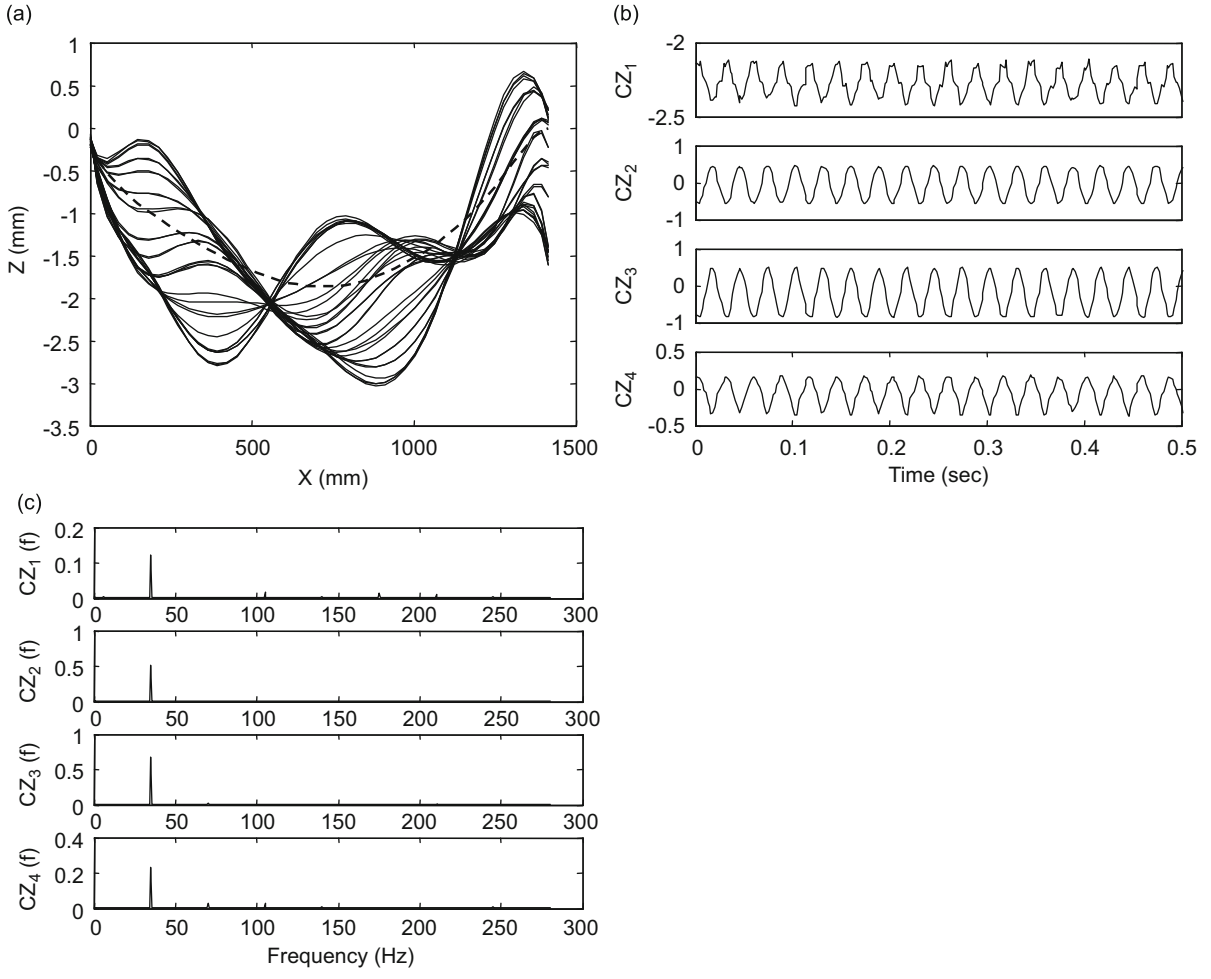

Fig. 16. Response to an excitation at Ω=35 Hz: (a) 32 curve-fitted consecutive vibration profiles within 0.055 s, (b) the modal coordinates of the *XZ*-plane vibration, and (c) the frequency spectra of the modal coordinates of the *XZ*-plane vibration.

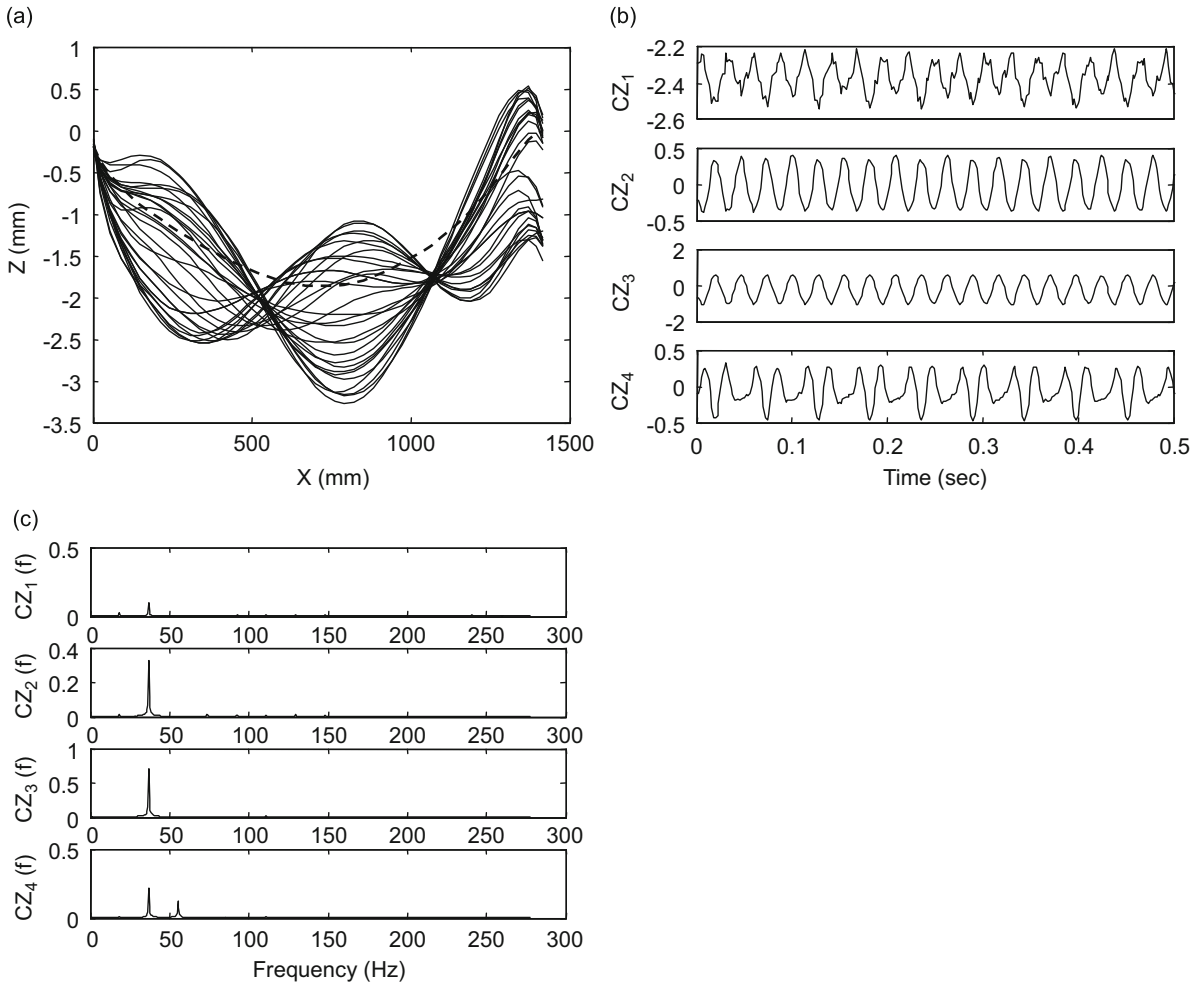

Fig. 17. Response to an excitation at Ω=37 Hz: (a) 30 curve-fitted consecutive vibration profiles within 0.052 s, (b) the modal coordinates of the *XZ*-plane vibration, and (c) the frequency spectra of the modal coordinates of the *XZ*-plane vibration.

17(b) and (c), and Fig. 18(b) and (c), one can see that the second and third modes are always in phase for all cases. Comparing the amplitudes of the second and third modes, one can see that the second-mode amplitude decreases and that of the third mode increases, indicating an increasing participation of the third mode. Because of linear modal coupling, the first mode is not negligible for responses to excitation at Ω=33 and 35 Hz, and the fourth mode is not negligible for responses to excitation at Ω=37 and 40 Hz. Traveling waves are evident in Fig. 16(a). Each profile appears to have a different maximum deflection location.

3.4.7. Responses of the sixth branch (B6)

The B6 branch in Fig. 6(b) and (c) has nonplanar responses similar to those of the B2 and B4 branches, but they are primarily composed of the third mode. The amplitudes of these higher-mode vibrations are smaller than those of the lower-mode vibrations of the B2 and B4 branches. Consequently, the measured vibration profiles have relatively lower precision. Fig. 19 (a) shows vibration profiles when the taut cable was excited at Ω=50 Hz. Respectively, they are plot of 22 consecutive curve-fitted vibration profiles within 0.038 s (a), the trajectory of Marker 8 (b), the modal coordinates (c, e), and the corresponding frequency spectra (d, f) of the *XZ*- and *XY*-plane vibrations. Both cases are typical responses of the B6 branch. It is obvious that the major components of the vibrations in both planes are the third mode. As the excitation frequency increases, the fourth mode may be excited by linear modal coupling because of the closeness of the excitation frequency to the fourth natural frequency. Fig. 20 shows a complex vibration when the taut cable was excited at Ω=53 Hz. Respectively, the plots are 20 consecutive curve-fitted vibration profiles within 0.036 s (a), the trajectory of Marker 8 (b), the frequency spectra (c, d) of *Z*- and *Y*-direction vibration of Marker 8, the modal coordinates (e, g), and the corresponding frequency spectra (f, h) of the *XZ*- and *XY*-direction vibration. Fig. 20(c) and (d) show that both *Z*- and *Y*-direction vibration of Marker 8 contain high-frequency harmonics with small but not negligible amplitudes. Four modes may not be enough for an accurate modal decomposition of this high-frequency vibration. From Fig. 20(e) and (f), it can be seen that the

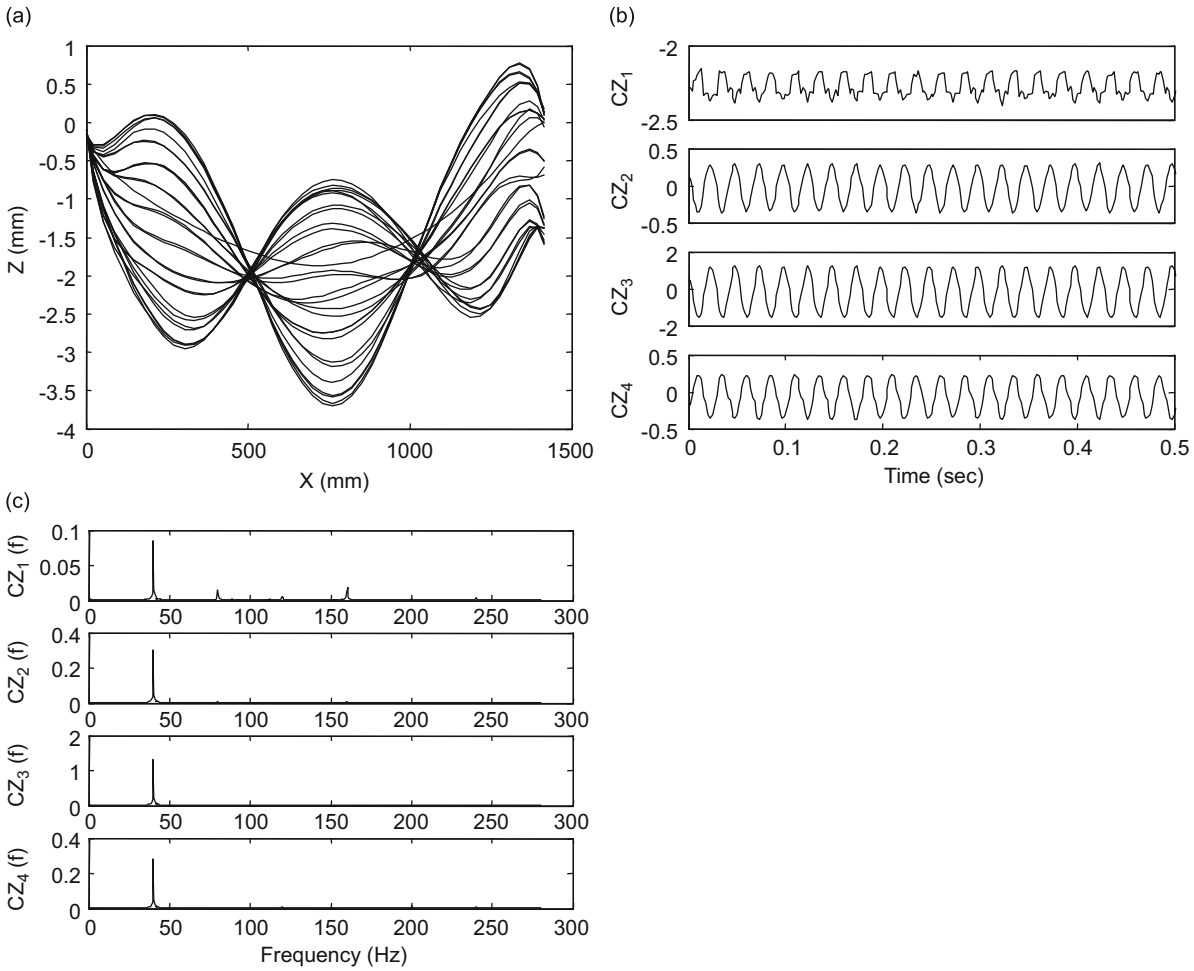

Fig. 18. Response to an excitation at Ω=40 Hz: (a) 28 curve-fitted consecutive vibration profiles within 0.048 s, (b) the modal coordinates of the *XZ*-plane vibration, and (c) the frequency spectra of the modal coordinates of the *XZ*-plane vibration.

in-plane vibration amplitudes of the third and fourth modes exhibit small differences. The vibration is dominated by the third mode and, therefore both nodes are clear in the *XZ*-plane vibration profile. From Fig. 20(g) and (h), it can be seen that the out-of-plane vibration amplitude of the third mode is much larger than other contributing modes. The vibration is dominated by more than one mode, making the nodes of the vibration profiles unclear. The right node, which is even more blurred than the left one, is close to the excitation support and, therefore, more influenced by the support displacement. This is especially pronounced for vibrations of higher modes because they have small amplitudes. Fig. 20(e) and (g) show the phase difference between the two major participating components, the third and fourth modes, of the *XZ*- and *XY*-plane vibrations. It can be seen that the phase difference between the third and fourth modal coordinates changes with the excitation frequency, indicating that these two linear modes move independently and cannot be combined into one nonlinear normal mode.

3.4.8. Responses of the seventh branch (B7)

The solution of the branch B7 was not studied in detail, because the shaker was often out of control for excitations in this frequency range, and only three different excitation tests were performed and recorded. Fig. 21 shows the responses when the taut cable was excited at Ω=50 Hz. Twenty-two consecutive curve-fitted vibration profiles within 0.038 s shown in Fig. 21(a) are clearly separated because the vibration was periodic. The number of separated profiles of the left half of the taut cable is different from that of the right half, indicating that the vibration consists of both symmetric and anti-symmetric modes. Fig. 21(b) and (c), the modal coordinates and corresponding frequency spectra for the *XZ*-plane vibration, show that the vibration were dominated by the third and fourth linear normal modes and that these two major components were in phase. The contribution of the second linear mode to the vibration was small and its phase was 180° different from those of the third and fourth modes. The contribution of the first linear normal mode was primarily due to the gravity-induced sag. For higher-mode vibrations, the influence of gravity and initial curvature on the natural frequency

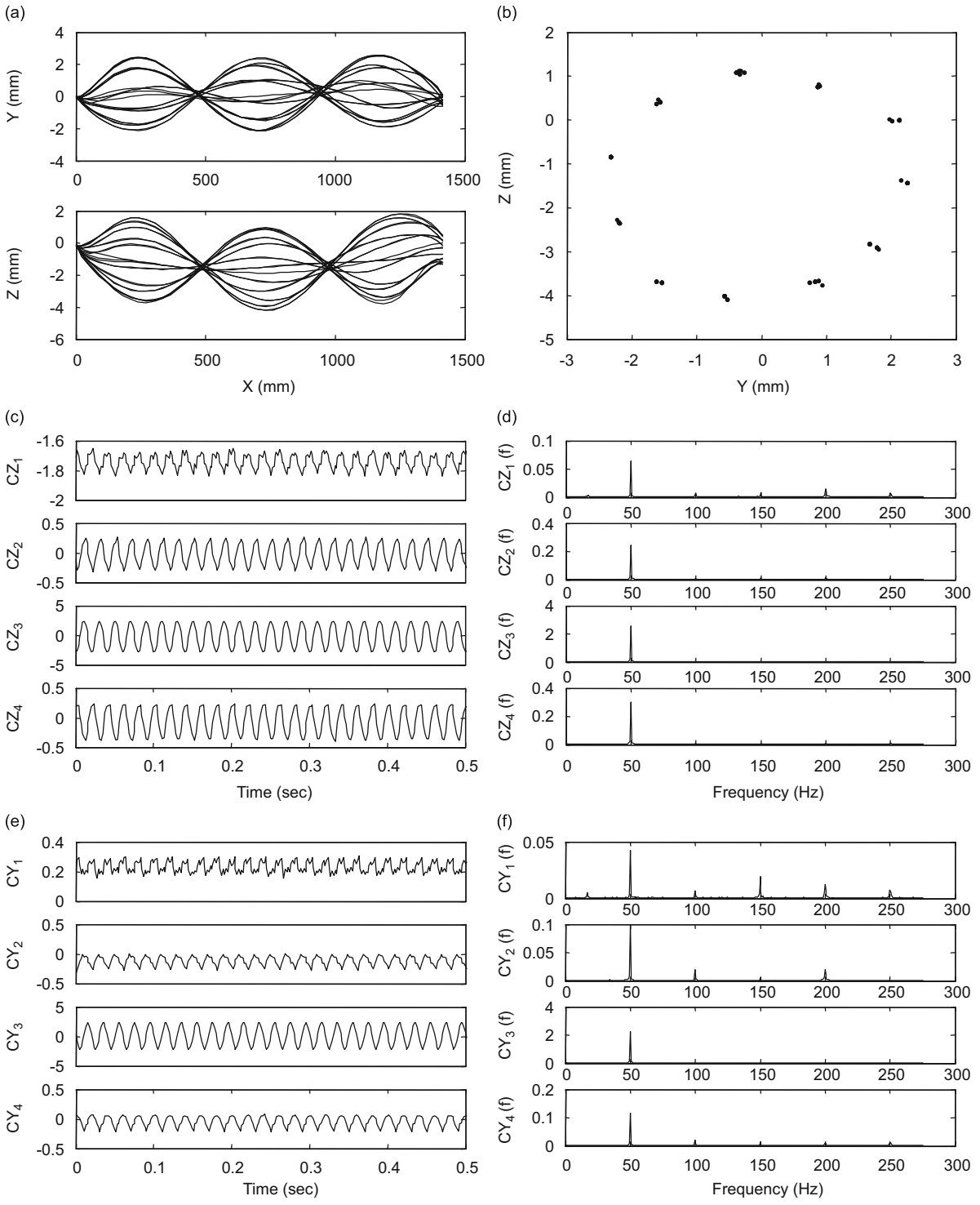

Fig. 19. Response to an excitation at Ω=50 Hz: (a) 22 curve-fitted consecutive vibration profiles within 0.038 s, (b) the trajectory of Marker 8, (c) the modal coordinates of the *XZ*-plane vibration, (d) the frequency spectra of the modal coordinates of *XZ*-plane vibration, (e) the modal coordinates of the *XY*-plane vibration, and (f) the frequency spectra of the modal coordinates of the *XY*-plane vibration.

decreases. This can be explained by the well-known crossover phenomena of natural frequencies of cables [1,15]. Taut cable has non-zero small sag and a small elasto-geometric parameter. Only natural frequencies of low-order in-plane symmetric modes are affected by the sag, while those of high-order modes stay nearly unchanged. Commensurate relationships between natural frequencies of higher in-plane and out-of-plane modes still exist and it is possible for

various resonances to occur. Therefore, additional linear normal modes are necessary for an accurate modal decomposition analysis of high-frequency vibrations.

4. Conclusions and discussions

This paper presents an experimental study of the nonlinear vibration of taut cables with small but not negligible sags using a 3-D motion analysis system. The taut cable studied was not as tensioned as ideal string or as loose as most widely studied cable with frequency–crossover related dynamic characteristics. As expected, dynamic characteristics of both string and cable were observed. The modal transitional vibration and compound modal vibration within a wide frequency range of the nonlinear vibration of taut cable was experimentally investigated. A practical and efficient frequency sweeping scheme for the frequency response study using the 3-D motion analysis system was developed. These experiments successfully recorded the planar and nonplanar/whirling vibration, hardening effect, and modal coupling vibration. The hysteretic phenomenon of response was also observed. The recorded frequency response clearly showed the sudden loss of stability of one branch and the jumping to another branch with increasing and decreasing frequency sweeps. For all cases, linear coupling excited neighboring modes. For some cases, phase differences between various participating modes changed as the excitation frequency changed, which indicated that those modes moved independently and therefore could not be combined into one nonlinear normal mode. The concept of nonlinear normal mode is thus questionable for application in the modal decomposition of taut cable nonlinear vibration.

Two types of responses observed. The first type was planar vibration primarily composed of two neighboring modes; it represented a transition phase from the lower mode to the next one. As the excitation frequency increased, the amplitude

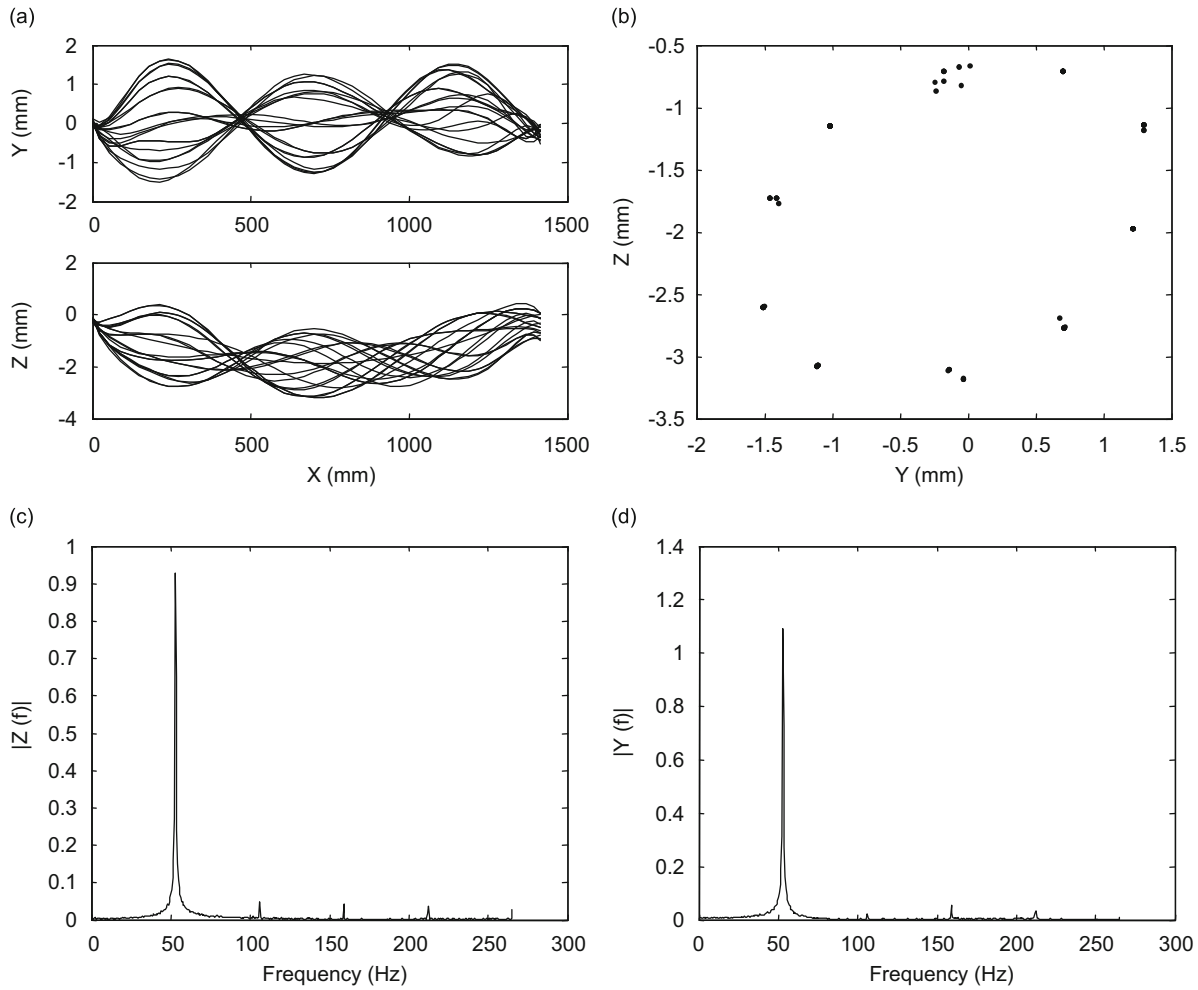

Fig. 20. Response to an excitation at Ω=53 Hz: (a) 20 consecutive curve-fitted consecutive vibration profiles within 0.036 s, (b) the trajectory of Marker 8, (c) the frequency spectra of *Z*-direction vibration of Marker 8, (d) the frequency spectra of the *Y*-direction vibration of Marker 8, (e) the modal coordinates of the *XZ*-plane vibration, (f) the frequency spectra of the modal coordinates of *XZ*-plane vibration, (g) the modal coordinates of the *XY*-plane vibration and (h) the frequency spectra of the modal coordinates of the *XY*-plane vibration.

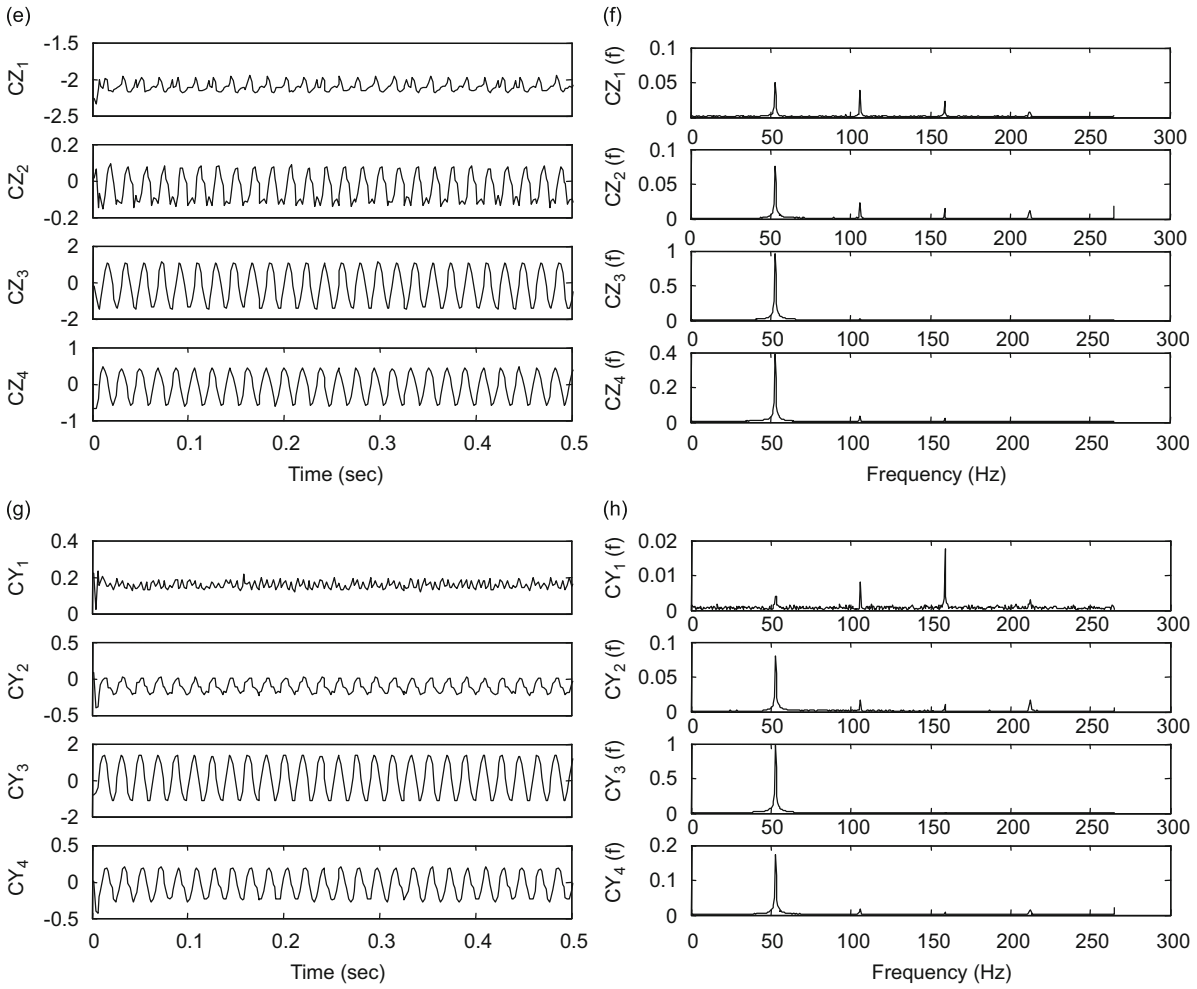

Fig. 20. (*Continued*)

of the lower one decreased while that of the other increased. These two linearly coupled modes were always in-phase or out-of-phase. Lower and higher modes may have been excited because of linear coupling, making the vibration more complicated. The first type of response is represented by the odd numbered branches shown in Fig. 6(b) and (c). The second type of response was a nonplanar vibration primarily composed of a single mode for both in-pane and out-of-plane responses. However, in certain cases, other modes may have participated in both planar and nonplanar vibrations because of linear and nonlinear coupling, making the vibration profile complex and irregular, although these modes have relatively small amplitudes in most cases. The second type of response is represented by the even numbered branches shown in Fig. 6(b) and (c).

Nonlinearities played critical roles in the nonlinear properties of the responses observed in this experimental study. Observed nonlinear phenomena include hardening effect, hysteretic phenomena, appearance of out of plane response to in-plane excitation, the resonance between different modes, etc. Theoretically, quadratic nonlinearity due to curvature and cubic nonlinearity due to cable stretching are both expected to be pronounced in the nonlinear dynamics of a taut cable. Recorded resonant responses such as 2:1 vibration were due to the intrinsic quadratic nonlinearity of the system. Since steel cable, which has high tension stiffness, was used for the experiments, stretching during oscillation was almost negligible and therefore, phenomena due to cubic nonlinearity were not observed.

The classic nonlinear vibration of ideal string is a weakly nonlinear problem and applicable methods, such as the multiple-scale method, can produce a fairly accurate theoretical prediction for experimental responses. This has been verified by some well-known research on this topic [11]. Typically, studies on nonlinear string vibration focus on the response to excitations with small frequency detuning around specified natural frequencies of the linear string. Compared to the vibration of ideal string examined in most theoretical studies, the taut cable experimentally studied in this paper vibrates with relatively large amplitudes. The examined excitation varied over a wide range (the first several natural frequencies) instead of a small range with small detuning around specified natural frequencies as applied in most weakly nonlinear analyses. The contributions, both of linearly and nonlinearly participating modes, were observed and

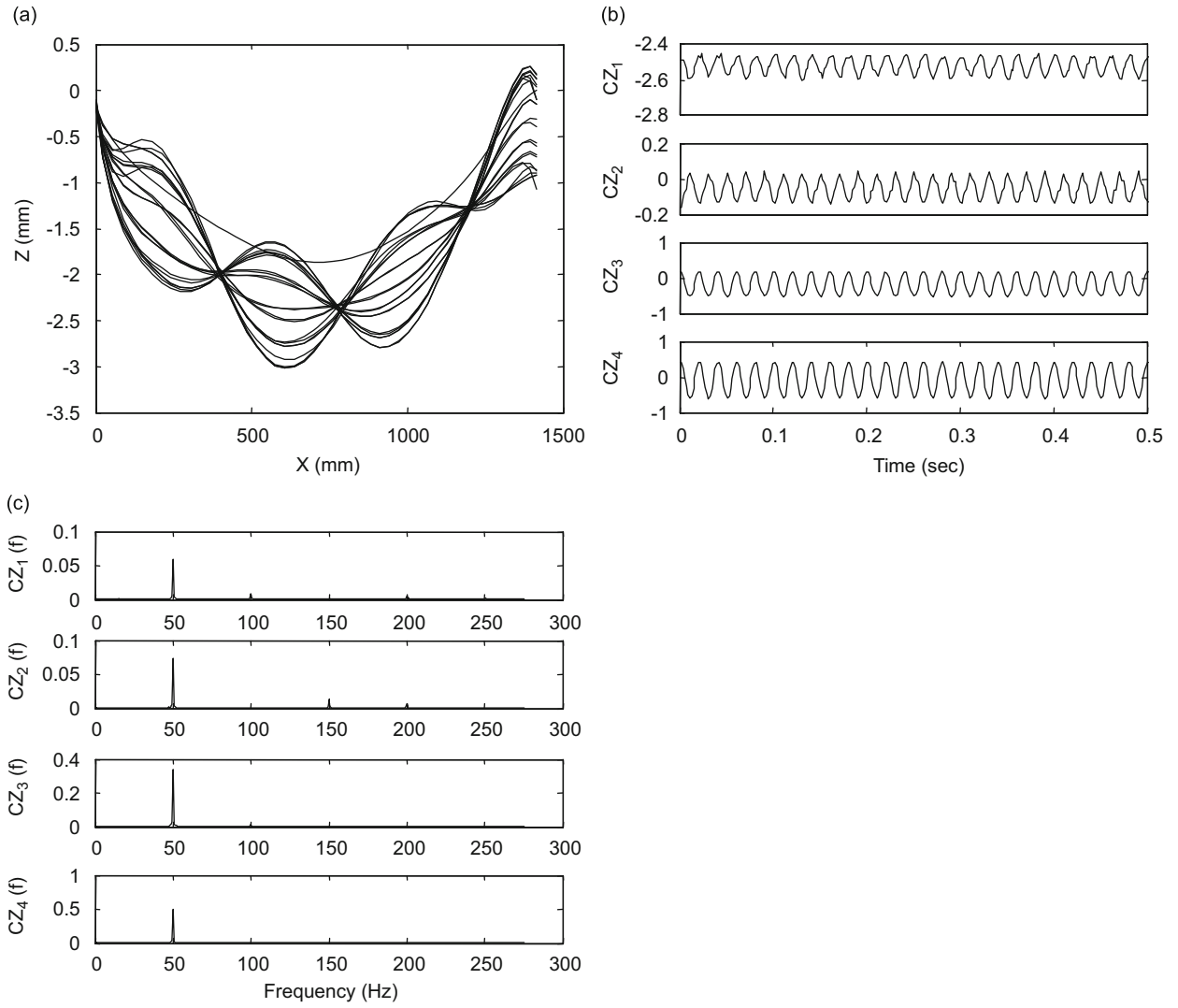

Fig. 21. Response to an excitation frequency at $\Omega = 50$ Hz. (a) 22 curve-fitted consecutive vibration profiles within 0.038 s, (b) the modal coordinates for the *XZ*-plane vibration and (c) the frequency spectra of the modal coordinates for the *XZ*-plane vibration.

investigated. Moreover, taut cable is not an ideal cable or string without any bending stiffness. At the support ends of the taut steel cable, both the bending and torsional stiffnesses are not negligible and it is more appropriate to be considered as a rod. It has been shown that in this kind of cable [17], the static profile differs from that of equivalent ideal cable or string at locations close to the end support because of bending stiffness. Accordingly, it can be confidently concluded that the influences of boundary bending and torsional stiffnesses on the dynamic response would also be not negligible. Therefore, a weakly nonlinear analysis of ideal cable or string may not be adequate for a reliable vibration response prediction study. A more accurate model together with more robust numerical analysis is believed to be the prerequisite for achieving this objective.

References

[1] H.M. Irvine, T.K. Caughey, The linear theory of free vibration of a suspended cable, *Proceedings of the Royal Society of London, Series A, Mathematical and Physical Sciences, England* 341 (1626) (1974) 299–315.
[2] C.V. Raman, The small motion at the nodes of a vibrating string, *Nature* 82 (1909) 9–19, doi:10.1038/082009b0.
[3] C.V. Raman, Oscillations of the stretched strings, *Journal of Indian Mathematical Club* 1 (1910) 14–19.
[4] C.V. Raman, Some remarkable cases of resonances, *Physics Review* 35 (1912) 449–458.
[5] C.V. Raman, Experimental investigation on the maintenance of vibrations, *Bulletin of the Indian Association for the Cultivation of Science* 6 (1912) 1–40.
[6] C.V. Raman, On the mechanical theory of the vibrations of bowed strings and of musical instruments of the violin family, with experimental verification of results—Part 1, *Bulletin, Indian Association for the Cultivation of Science*, 1918.
[7] J. Woodhouse, P.M. Galluzzo, The bowed string as we know it today, *Acta Acustica United with Acustica* 90 (2004) 579–589.
[8] J.M. Johnson, A.K. Bajaj, Amplitude modulated and chaotic dynamics in resonant motion of strings, *Journal of Sound and Vibration* 128 (1989) 87–107.

[9] A.K. Bajaj, J.M. Johnson, On the amplitude dynamics and crisis in resonant motion of stretched strings, *Philosophical Transactions of the Royal Society of London* 338 (1649) (1992) 1–41.
[10] T.C. Molteno, N.B. Tufillaro, An experimental investigation into the dynamics of a string, *American Journal of Physics* 72 (9) (2004) 1157–1169.
[11] S.A. Nayfeh, A.H. Nayfeh, D.T. Mook, Nonlinear response of a taut string to longitudinal and transverse end excitation, *Journal of Vibration and Control* 1 (1995) 307–334.
[12] P.F. Pai, *Highly Flexible Structures: Modeling, Computation and Experimentation*, AIAA, Reston, VA, 2007.
[13] S. Ramanathan, J. Hu, P.F. Pai, Experimental nonlinear mechanics of highly flexible structures using a 3-D motion analysis system, *Proceedings of the Seventh International Conference on Motion and Vibration Control*, St. Louis, MO, August 8–11, 2004.
[14] J. Hu, Nonlinear Mechanics and Testing of Highly Flexible One-dimensional Structures Using a Camera-based Motion Analysis System, PhD Thesis, Department of Mechanical and Aerospace Engineering, University of Missouri, Columbia, 2006.
[15] M.S. Triantafyllou, Linear dynamics of cables and chains, *The Shock and Vibration Digest* 16 (3) (1984) 9–17.
[16] P.F. Pai, S.Y. Lee, Nonlinear structural dynamics characterization using a scanning laser vibrometer, *Journal of Sound and Vibration* 264 (2003) 657–687.
[17] G. Bowden, Stretched wire mechanics, *Proceedings of the Eighth International Workshops on Accelerator Alignment (IWAA 2004)*, Geneva, Switzerland, October 4–7, 2004.